HHS Public Access

Author manuscript

Neuron. Author manuscript; available in PMC 2022 November 03.

Published in final edited form as:

Neuron. 2021 November 03; 109(21): 3473–3485.e5. doi:10.1016/j.neuron.2021.08.004.

Bottom-up inputs are required for the establishment of top-down connectivity onto cortical layer 1 neurogliaform cells

Leena Ali Ibrahim[1,2], **Shuhan Huang**[1,2,3], **Marian Fernandez-Otero**[1,2], **Mia Sherer**[1,6], **Yanjie Qiu**[1,2], **Spurti Vemuri**[6], **Qing Xu**[5], **Robert Machold**[4], **Bernardo Rudy**[4], **Gord Fishell**[1,2,*]

[1]Harvard Medical School, Blavatnik Institute, Department of Neurobiology, Boston, MA, USA.

[2]Broad Institute, Stanley Center for Psychiatric Research, Cambridge, Massachusetts, USA.

[3]Program in Neuroscience, Harvard Medical School, Boston, Massachusetts, USA.

[4]Neuroscience Institute, New York University School of Medicine, NY, USA.

[5]Center for Genomics & Systems Biology, New York University, Abu Dhabi, UAE.

[6]Northeastern University, Boston, MA, USA

Abstract

Higher order projections to sensory cortical areas converge on layer 1 (L1), the primary site for integration of top-down information via the apical dendrites of pyramidal neurons and L1 GABAergic interneurons. Here, we investigated the contribution of early thalamic inputs onto L1 interneurons for the establishment of top-down connectivity in the primary visual cortex. We find that bottom-up thalamic inputs predominate during L1 development and preferentially target neurogliaform cells. We show that these projections are critical for the subsequent strengthening of top-down inputs from the anterior cingulate cortex onto L1 neurogliaform cells. Sensory deprivation or selective removal of thalamic afferents blocked this phenomenon. While early activation of the anterior cingulate cortex resulted in a premature strengthening of these top-down afferents, this was dependent on thalamic inputs. Our results demonstrate that proper establishment of top-down connectivity in the visual cortex depends critically on bottom-up inputs from the thalamus during postnatal development.

*Lead Contact: G.F. (gordon_fishell@hms.harvard.edu).

AUTHOR CONTRIBUTIONS

LAI and GF conceived the project and wrote the manuscript. LAI performed experiments and analysis. SH carried out dLGN injections, recording and analysis. MFO, YQ and SV assisted with histology experiments. MS, YQ and SV assisted with tiling scope imaging and rabies quantification. MS assisted with Neurolucida reconstructions. QX produced some of the viruses used in the study (labeled as NYUAD). RM and BR contributed to the design of the experiments and discussion.

INCLUSION AND DIVERSITY STATEMENT

One or more of the authors of this paper self-identifies as an underrepresented ethnic minority in science. One or more of the authors of this paper self-identifies as a member of the LGBTQ+ community. One or more of the authors of this paper self-identifies as living with a disability. While citing references scientifically relevant for this work, we also actively worked to promote gender balance in our reference list.

COMPETING INTERESTS

G.F. is a founder of Regel. All other authors declare no competing interests.

eTOC blurb

During development in the visual cortex, there is a shift in the flow of information processing from predominately bottom-up to top-down. Ibrahim et al show that the strength of thalamic inputs onto layer 1 interneurons directly impacts the development of connectivity of these cells from the anterior cingulate cortex.

Introduction

Our capacity to perceive and react to a rapidly changing world relies on the ability of the neocortex to respond accurately and precisely to sensory stimuli in a dynamic environment. Processing sensory information such as vision, depends critically on our ability to attend to stimuli, filter distractors, and accurately make predictions about our surroundings (Desimone and Duncan 1995, Rao and Ballard 1999, Kastner and Ungerleider 2000, Ardid, Wang et al. 2007, Squire, Noudoost et al. 2013, Zhang, Xu et al. 2014, Huda, Sipe et al. 2020). The integration of top-down feedback from higher order brain areas and incoming sensory signals allows for such functions. Cortical inhibitory interneurons (INs) have been increasingly implicated in this process. While parvalbumin (PV), somatostatin (SST), and vasoactive intestinal peptide (VIP) INs have been posited to contribute to such computations (Lee, Kruglikov et al. 2013, Fu, Tucciarone et al. 2014, Zhang, Xu et al. 2014, Leinweber, Ward et al. 2017, Schneider, Sundararajan et al. 2018), the involvement of L1 INs has been less explored. L1 contains dense axonal projections from various brain regions and is in fact, the main target of cortico-cortical projections from diverse cortical areas, as well as thalamocortical projections (Oh, Harris et al. 2014, Zingg, Hintiryan et al. 2014, Schuman, Dellal et al. 2021). These projections not only target the distal apical dendrites of pyramidal neurons, but also the INs located within L1 (Ibrahim, Schuman et al. 2020). Importantly, L1 INs have been shown to receive both thalamic (Ji, Zingg et al. 2015) and inter-cortical connections (Leinweber, Ward et al. 2017, Cohen-Kashi Malina, Tsivourakis et al. 2021, Naskar, Qi et al. 2021). This ideally positions them to modulate incoming sensory inputs and regulate excitatory responses (Zhu and Zhu 2004, Jiang, Wang et al. 2013, Lee, Wang et al. 2015, Anastasiades, Collins et al. 2020, Cohen-Kashi Malina, Tsivourakis et al. 2021). L1 INs have also been shown to play a role in cross-modal integration (Ibrahim, Mesik et al. 2016), interhemispheric inhibition (Palmer, Schulz et al. 2012), associative fear learning and plasticity (Abs, Poorthuis et al. 2018, Pardi, Vogenstahl et al. 2020), as well as sensory motor integration (Mesik, Huang et al. 2019). Taken together, these findings implicate L1 INs as a critical nexus for the integration of bottom-up and top-down signaling.

A considerable breadth of evidence supports the idea that activity in the early postnatal cortex is initially dominated by bottom-up signals. The cortex only later develops recurrent activity following the establishment of functional connectivity between primary and associative cortical areas (Colonnese, Kaminska et al. 2010, Luhmann and Khazipov 2018, Dominguez, Ma et al. 2021). These findings suggest that the emergence of cortical function is a sequential process that relies on distinct epochs of activity. While it is well established that sensory experience plays a crucial role in excitatory and inhibitory neuron development (Chou, Babot et al. 2013, Pouchelon, Gambino et al. 2014, De Marco García, Priya et al. 2015), whether it is required for the establishment of top-down circuits is not known.

The two largest populations of L1 INs are the neurogliaform (NGF) and “canopy” cells, both of which express the neuron-derived neurotrophic factor (NDNF; (Schuman, Machold et al. 2019). In this paper, we explore the development of the afferent connectivity to these cell types in the primary visual cortex (V1) and reveal that they exhibit significant differences in when they receive afferent inputs. Using monosynaptic rabies tracing, we find that bottom-up thalamic inputs dominate during development, whereas top-down inputs are progressively strengthened later in development. Our results show that early in development, L1 NGF cells are the main recipients of thalamic inputs. By contrast, the canopy cells in L1 only receive thalamic afferents at later ages. Moreover, we find that bottom-up inputs from the dorsal lateral geniculate nucleus (dLGN) onto L1 NGF cells are required for the later establishment of cortico-cortical top-down afferents from the anterior cingulate cortex (ACC). This region that has been implicated in visual discrimination (Zhang, Xu et al. 2014, Huda, Sipe et al. 2020) and visuo-motor mismatch responses (Attinger, Wang et al. 2017, Leinweber, Ward et al. 2017) through their projections to V1. Specifically, we observe that enucleation or ablation of thalamic inputs to L1 INs prevents the strengthening of ACC afferents onto them. Conversely, premature activation of the ACC inputs results in precocious development of ACC input strength onto NGF cells, a phenomenon that is critically dependent on the thalamus. Altogether, these findings demonstrate the importance of bottom-up thalamic inputs on the development of top-down connectivity from the ACC onto L1 NGF INs in V1.

Results

Developing L1 INs switch from receiving predominantly bottom-up thalamic to receiving top-down cortico-cortical afferents.

To map L1 INs’ monosynaptic afferent connectivity, we used the *NDNF-dgCre* driver mouse line (Tasic, Menon et al. 2016) to label both canopy and L1 NGF cells, which together constitute ~70% of L1 INs (Tasic, Yao et al. 2018, Schuman, Machold et al. 2019, Ibrahim, Schuman et al. 2020). In combination with a *Cre*-dependent AAV-helper virus and a genetically modified CVS N2c strain of the G-deleted rabies (N2c-RV) (Fig.1A), we surveyed the monosynaptic input connectivity of these cells. This rabies strain has been found to be both less toxic and more efficient in retrograde labeling of presynaptic cells than the originally used B19 version (Wickersham, Lyon et al. 2007, Reardon, Murray et al. 2016). Cre-dependent expression of the AAV helper virus in NDNF cells provided the necessary components for the infection of EnvA-pseudotyped rabies virus (TVA receptor), as well as for its replication and transport (G protein) (Fig. 1A). All the required helper components (i.e., N2C-G protein, TVA receptor and eGFP reporter) were contained within a single AAV virus (Pouchelon 2020). AAV-helper and N2C-RV-mCherry (RV) viruses were co-injected in V1. As expected, the starter cells (eGFP and mCherry co-expressing cells) were primarily localized within L1 (Fig.1B and Fig S1A). We used this approach at both developmental and adult timepoints to compare the monosynaptic afferents onto L1 INs in V1.

To assess developmental connectivity, we injected the AAV helper and N2c-RV at P1 and analyzed the retrogradely labeled cells at P15. For the adult connectivity, we injected

mice at 4–5 weeks of age and analyzed the brains similarly two weeks later (Fig. 1C). By quantifying the normalized number of retrogradely labeled neurons across regions (see Methods for details), we found that during development, the most numerous inputs that L1 INs receive were from the sensory thalamus, (i.e., dLGN, Fig.1D–E; 0.471± 0.0217). In contrast, in adults, while L1 INs maintained thalamic inputs, they were collectively less numerous than the long-range cortico-cortical inputs from the anterior cingulate (ACC), premotor cortex (M2) and the retrosplenial (RSP) cortex (Fig. 1E left panel; bottom-up proportion: 0.133±0.016 vs top-down proportion: 0.478±0.011). Interestingly, we found that ACC inputs increased more strongly from development to adulthood (~5-fold increase) compared to inputs from the RSP (~2-fold increase) (Fig. 1E right panel). We focused on these projections, as they have been shown to have abundant axonal arbors in the superficial layers of V1. The increase in long-range cortico-cortical connectivity in the adult indicates that as L1 INs mature, their afferents shift from being predominantly bottom-up to top-down. Additionally, L1 INs in V1 received both local inputs, primarily from L5 and L6 (predominantly L6b) during development (Fig. S1B top and see (Meng 2020); from L5 (pyramidal neurons and presumably SST INs, Fig. S1B (bottom), (Abs, Poorthuis et al. 2018)) in the adult, as well as long-range cortical inputs from higher visual areas (V2L/M), auditory cortex (AUD) and posterior parietal cortex (PTLp) (Fig 1F and see (Cohen-Kashi Malina, Tsivourakis et al. 2021). Interestingly, we observed a smaller but consistent projection to NDNF+ L1 INs from the contralateral ectorhinal cortex and ipsilateral claustrum. Furthermore, NDNF+ L1 INs received a small number of afferents from both the basal forebrain and hypothalamic nuclei (Fig 1F).

NDNF+ L1 INs also received inputs from diverse thalamic nuclei (Fig 1F) such as the group of anterior thalamic nuclei (ATN) as well as the anterior pretectal nucleus (APN). Inputs from higher order visual thalamic nuclei, such as the lateral-posterior (LP) nucleus and other visual thalamic nuclei such as the lateral-dorsal (LD) (Nassi and Callaway 2009, Saalmann, Pinsk et al. 2012) were also very prominent. Interestingly, while LP is thought to be the main source of thalamic inputs to L1 in V1 (Roth, Dahmen et al. 2016); based on our rabies tracing data, we found that the dLGN inputs were more predominant onto NDNF+ cells both during development and in the adult (Fig. S1C top and bottom).

L1 NGF cells and L4 excitatory cells receive dLGN inputs, some of which are shared

To label bottom-up thalamic afferents, we utilized the *Vipr2-Cre* driver line, which has been previously shown to be specifically expressed in the dLGN, and not in LP (Zhuang 2019). *Vipr2-Cre* mice crossed with the tdTomato reporter Ai14 labels the dLGN, (but not LP), the ventro-basal nucleus (VB) (Fig.2A), and the ventral medial geniculate body (MGBv); i.e., the visual, somatosensory, and auditory sensory nuclei in the thalamus, with a high degree of specificity during both development and in the adult. To determine the strength of thalamic inputs to L1 INs in V1, we injected Cre-dependent channelrhodopsin (AAV1-EF1a-DIO-hChR2-eYFP) in the dLGN and as expected thalamic fibers were observed within both L4 (the main recipient of dLGN inputs) and L1 of V1 (Fig. 2B). We injected neonatal P0/P1 mouse pups, or adult mice, and after a two-week survival period, we performed whole cell voltage clamp recordings from both L1 and L4 neurons in V1 coronal slices in response to optogenetic stimulation of dLGN fibers in V1 (Fig. 2C).

We wanted to determine which L1 IN subpopulation is the recipient of dLGN inputs and to what extent these inputs overlap with those onto L4. It is well known that L1 INs are diverse. Historically they have been classified into two main groups: neurons with an axonal arbor mainly confined to L1, which include NGF cells (called elongated NGF cells by (Jiang, Wang et al. 2013) because their axonal arbor spans several columns); and cells with descending collaterals to deep layers called single bouquet cells (SBCs) (Kawaguchi and Kubota 1997, Zhu and Zhu 2004, Cruikshank, Ahmed et al. 2012, Jiang, Wang et al. 2013, Muralidhar, Wang et al. 2013). Schuman et al., recently showed that the neurons that have an axonal arbor largely confined to L1 express NDNF, a marker expressed in 70% of L1 INs. Furthermore, they showed that NDNF neurons consist of two subtypes: NGF neurons and a cell type they called “canopy” cells (Schuman, Machold et al. 2019). Despite their gross morphological similarities, the two subpopulations are distinct in their expression of Neuropeptide Y (NPY), intrinsic physiological properties and output connectivity. Specifically, NGF cells are NPY^+ (Fig S2A), late spiking and have a ramping-up membrane depolarization, with a relatively high rheobase and lower input resistance during development (Fig S2B left panel and Fig S2C. Also see Table 1 for other intrinsic physiological differences between development and adult). Canopy cells by contrast are regular spiking, display a small degree of spike adaptation and have a voltage sag in response to hyperpolarizing current injection (Fig S2B middle panel).

We wanted to determine whether these cell types receive thalamic inputs and if so, how the strength of these inputs compare to those targeting L4 excitatory cells (the main input thalamo-recipient layer). We found that NGF cells, but not canopy cells, receive considerable direct thalamic input (AMPA current recorded by clamping cells at −70mV) during development (Fig. 2D–E, NGF cell response: 97.3±8.8pA vs Canopy cell response: 11.63±2.5pA). Interestingly, in adults the responses on canopy cells became comparable to those of NGF cells (Fig. 2F). While in both development and adults the response of L4 excitatory neurons was on average twice that of L1 INs, in some instances NGF cell responses were comparable (Fig. 2G, (Takesian, Bogart et al. 2018). We also performed L1 and L4 recordings in WT mice injected with AAV-hSynh-ChR2-eYFP virus and found that the responses elicited were comparable to those found using the Vipr2-Cre line (Fig S3A–C). Notably the largest non NDNF population of L1 INs, the alpha-7 expressing L1 INs (Schuman, Machold et al. 2019) (Fig S2B, right panel), were found to barely receive any thalamic input in either development or in the adult (Fig 2E–F). Thus, across development the thalamic innervation of L1 INs is cell type specific.

Next, we wanted to determine whether the thalamic afferents that project to L1 are shared with those that project to L4. To that end, we utilized a L4-specific *Cre* driver line (*Scnn1a-Cre*) and used a modified rabies approach, where the RV also expresses *FlpO* recombinase together with mCherry. AAV helper and N2c-RV-FlpO-mCherry were co-injected in L4 of V1, followed by an injection of a flp-dependent hChr2-eYFP in the dLGN (Fig. 2H). This allowed us to examine the projection pattern of L4-projecting dLGN neurons by using an antibody against hChR2 to visualize the fibers in V1. In addition to their projection in L4, the retrogradely labeled dLGN neurons (Fig. 2J lower panel) were found to have collaterals in L1 (Fig. 2J, upper panel). This demonstrates L4 and L1 share a fraction of inputs from the same thalamic neurons. To independently confirm this, we sparsely labeled neurons

in the dLGN, by injecting an AAV carrying Cre recombinase in the contralateral retina. This virus travels anterogradely and trans-synaptically into the dLGN with a low efficiency (Zingg, Chou et al. 2017). This was followed by an injection of a Cre-dependent hChR2-mCherry AAV in the dLGN (Fig. 2K) and allowed us to directly visualize dLGN neurons that project to both L4 and L1 (Fig. 2L). After the tracing of these axonal arborizations (Fig. 2M), we found that there were bifurcating collaterals within both L4 and L1, at the single axon level (Fig. 2M middle panel). Those axons that projected to both L4 and L1 represented approximately 8% of all axons traced (L1 projecting only: 45/224 axons traced; L4 projecting only: 161/224; L1 and L4 shared axons: 18/224 axons traced) (Fig 2M right panel). This confirmed that small subset of thalamic axons targeted both layers, with the majority being either L4 or L1 targeting.

ACC, but not RSP inputs to L1 INs strengthen across development

To elucidate the corresponding developmental changes in the strength of top-down inputs, we focused on the projections from the ACC to V1, since they showed the most dramatic changes across development. In adults, inputs from the ACC have been shown to extensively arborize within L1 targeting various postsynaptic neurons across the different layers of V1 (Leinweber, Ward et al. 2017). However, the dynamics by which this input is established across development are unknown. To explore this question, we injected AAV-hSyn-hChr2-eYFP in the ACC region (Fig. 3A) and assessed the projection pattern (Fig. 3B) and input strength (Fig. 3C) in L1 and L2/3 of V1 both during development and in the adult. Based on our rabies tracing results, we expected to see fewer projections from the ACC to V1 during development (Fig.1D–E). However, as early as P10, ACC afferents were already observed to be distributed across the different layers of V1. Strikingly, these become concentrated within the superficial and the deep layers of V1 by adulthood (Fig. 3B and S4A). To assess the functional strength of these projections during development (P13-P15) and in the adult (~6–7 weeks), we optogenetically activated the ACC axons in V1 and recorded from the different L1 IN subtypes, as well as L2/3 excitatory cells (Fig. 3C). To ensure that the observed differences did not result from differential levels of hChR2 expression, both ages were examined two weeks post-injection. We found that during development, despite the abundance of fibers from the ACC to V1 (Fig S4A right panel), the amplitude of responses in both L1 and L2/3 neurons were small (Fig. 3D and 3E left panel, L1 NGF response: −32.075±2,56pA; L1 Canopy response: −19.66±1.314pA; L2/3 excitatory neuron response: −7.5±0.5pA). Responses in L1 were still on average greater than those observed in L2/3, a trend that becomes more pronounced in the adult (Fig.3E, right panel). Specifically, the peak amplitude of AMPA currents increased by ~10 fold in L1 INs by adulthood (Fig. 3F). Interestingly, L1 NGF cells were the main recipients of these inputs. While some of these differences in connectivity strength could be attributed to maturation of their intrinsic properties (Fig S2C and Table 1), the change in current amplitude likely reflects synaptic strengthening. By contrast, the inputs onto alpha-7 (data not shown) and canopy cells were considerably smaller and were roughly comparable to those found onto L2/3 excitatory cells (Fig. 3E; L1 NGF response: −171.6±3.03pA, L1 canopy response: −38.33±2.179pA, L2/3 excitatory neuron response: −21.75±1.03pA). Moreover, other INs in L2/3 also received ACC inputs (Zhang, Xu et al. 2014, Ma, Liu et al. 2021) but to a lesser degree compared to

L1 NGF cells (Fig S4C–D; PV response: −4.2±0.32pA; SST response: −13.8±1.35pA; VIP response: - 18.4±1.76pA).

Next, we wanted to determine if inputs from the RSP were similarly modulated across development. RSP has been shown to be involved in visual navigation (Makino and Komiyama 2015, Fischer, Mojica Soto-Albors et al. 2020, Mao, Molina et al. 2020), and we found it to be the other major source of cortico-cortical inputs to L1 INs in V1. Given that, compared to ACC, RSP connectivity is established earlier during development (Fig.1D–E), we predicted that it would follow a similar trend but to a lesser degree. Interestingly, although more variable, on average RSP projections (Fig S4E) remain unchanged across development, despite having similar cell type specificity (Fig 3G) in their L1 IN targeting (Fig 3H–I; L1 NGF response: −211±14.6pA (development); −134.5±11pA (adult), L1 canopy response: −19.63±1.2pA (development); −27.58±2.86pA (adult); L2/3 excitatory neuron response: −49.5±4.6pA (development; −34.35±3.12pA (adult). These results suggest that the developmental refinement and strengthening of connections from ACC, but not RSP to V1, is developmentally regulated and occurs in a progressive and cell-type specific manner.

L1 NGF cells require bottom-up sensory inputs for the strengthening of top-down connectivity from ACC

The observation that bottom-up sensory afferents onto L1 INs are established prior to their receipt of ACC inputs, prompted us to ask whether the developmental refinement of these inputs is dependent on sensory activity. To do so, we examined the impact of sensory deprivation on ACC afferent strengthening by performing early postnatal enucleation, (~P4), as well as later prior to eye opening (~P11) (Fig. 4A). We found that in the adult V1, enucleation resulted in a significant decrease in the strength of ACC inputs onto L1 NGF cells (Fig. 4C–D and E; Control response: −171.6±3.03pA; P4-enucleated response: −33.625+2.36pA; P11-enucleated response: −20.725+0.95pA). Interestingly, this did not result in any drastic morphological changes in L1 INs (Fig. 4B), but it did result in a small and significant decrease in their input resistance (Fig S5H). In addition, enucleation also results in an increase in the frequency of spontaneous excitatory events onto L1 INs, perhaps as a consequence of a compensatory increase in total excitatory inputs stemming from the enucleation (Fig.S5A–C) as seen in other cell types in the cortex (De Marco García, Priya et al. 2015, Frangeul, Kehayas et al. 2017). Furthermore, when we measured the failure rate of ACC inputs onto L1 NGF cells using a proxy to minimal stimulation (1ms long blue-light pulse), we observed a significant increase in failed trials in enucleated mice (Fig S5D), suggesting a change in synapse number. Notably, in enucleated animals, a similar reduction was not observed within L2/3 VIP INs, the second largest IN target of ACC inputs in L2/3 of V1 (Fig S5F; Control VIP response: 18.4±1.76pA; enucleated VIP response: −13.3±1.13pA), suggesting that these INs do not require sensory activity for the establishment of their ACC inputs.

Enucleation is also known to have indirect impact on other areas of the visual system (Williams, Reese et al. 2002, Nahmani and Turrigiano 2014, Rose, Jaepel et al. 2016, Jaepel, Hübener et al. 2017, Bhandari 2020, Hooks and Chen 2020). Indeed, we observed that

this procedure resulted in alteration of the dLGN structure itself (Fig S6A) as well as in the density of thalamic fibers within L1 becoming more diffuse. Moreover, monosynaptic rabies tracing from L1 NDNF+ INs demonstrated that while there was no net change in the connectivity from the thalamus, there is a decrease in dLGN connectivity coupled with a corresponding increase in LD and LP afferents (Fig S6C). Using optogenetic stimulation of hChR2 expressing fibers from enucleated (P4 and P11) *Vipr2-Cre* mice, we observed a decrease of dLGN input strength onto L1 NGF cells (Fig S6B). Interestingly, while the thalamic afferents to L4 excitatory neurons were marginally reduced, their impact on L1 NGF cells was more dramatic. To examine whether a less invasive disruption to sensory input had a similar effect on ACC to L1 connectivity, we subjected the mice to dark rearing (starting at P4). Similar to enucleation, we observed a decrease of ACC input strength onto NGF cells (Fig 4E) as well as an increase in the failure rate in the transmission of these inputs (Fig S5D). Interestingly, enucleation did not result in a change of RSP inputs onto NGF cells in L1 (Fig S5G).

Next, we wanted to confirm if general sensory activity or direct thalamic inputs to L1 are needed for the strengthening of ACC inputs across development. To do so, we injected AAV helpers together with RV-FlpO-mCherry virus in *NDNF-dgCre* pups followed by an injection of a *Flp*-dependent diphtheria toxin subunit A (DTA) in the dLGN (Fig. 4F). This allowed us to selectively ablate only those dLGN neurons that innervate L1 INs (Fig. 4G), with the caveat that the common inputs between L4 and L1 will also be disrupted (which represent only 8% of the thalamic inputs to L4). Importantly the RV-infected L1 INs remain physiologically healthy up to 5 weeks post rabies infection (data not shown and see (Reardon, Murray et al. 2016)). Upon reaching adulthood, AAV-hSyn-hChR2-eYFP virus was injected into the ACC and following a two-week survival period the RV-injected starter cells were recorded in V1. Similar to what was observed in the sensory deprivation experiments, we found a significant decrease in the strength of the ACC inputs onto L1 INs (Fig. 4H). Here, the response amplitude was normalized to that observed in control non-sensory deprived animals. These results suggest that bottom-up sensory inputs are required for the strengthening of projections from the ACC onto L1 NGF cells in V1.

Top-down connectivity onto L1 NGF cells depends upon coordination with bottom-up inputs

Given that compromising bottom-up sensory signaling prevents the strengthening of ACC inputs onto L1 NGF cells in V1, we wondered whether early activation of either dLGN or ACC inputs would result in the premature strengthening of the latter. To explore this question, in two separate cohorts of pups, we injected the dLGN of *Vipr2-Cre* mice (~P1) with an AAV-DIO-hM3D(Gq)-DREADD-mCherry or the ACC with a AAV-hM3D(Gq)-DREADD-mCherry (Fig. 5A–B). In both circumstances, to measure the strength of top-down inputs, we also injected hChR2-eYFP in the ACC. In the case of ACC-Gq-DREADD activation, we found that at least 70% of the ACC neurons expressed both mCherry and eYFP, along with responding to both optogenetic and chemogenetic activation (Fig S7A–C).

We then compared the strength of ACC projections onto L1 INs in these two experimental groups at ~P14, following daily injections of Clozapine-N-oxide (CNO) or saline (starting

at P5, Fig. 5C). In comparison with developmental controls (from Fig 3E), we did not observe strengthening of ACC projections onto L1 INs when the dLGN pathway was over-activated (Fig. 5D–E). In contrast, selective activation of the ACC pathway (CNO starting at either P5 or P11) resulted in a significant increase in the ACC input strength onto L1 INs cells compared to either saline or CNO injected control groups (Fig. 5F–G and Fig S7D). Moreover, this increase was specific to the NGF cell population, and was not observed in canopy, a7 or L2/3 excitatory neurons (Saline control response: −34.38±3.72pA and CNO control response: −42.81±2.94pA vs Gq-DREADD-ACC (CNO starting at P5) NGF cell response: −163.529±6.84pA, Gq-DREADD-ACC (CNO starting at P11) NGF cell response: −164.22±9.55pA; Gq-DREADD-ACC Canopy cell response: −17.4±2.08pA, Gq-DREADD-ACC L2/3 response: −11.4±0.55pA). On average there was a ~4-fold increase in the strength of ACC inputs to NGF cells following ACC-Gq-DREADD activation. This was coupled with a decrease in the percentage of failed trials in response to a 1ms blue-light pulse (~32.5% in saline/CNO control vs ~12% in Gq-DREADD ACC activated mice) (Fig S7E). While the premature increase in strength could be attributed to a general plasticity mechanism, the cell-type specificity of this increase was very striking.

We wondered whether this augmentation in the strength of ACC afferents to L1 NGF cells was dependent upon bottom-up sensory thalamic signals. We reasoned that this may occur due to the coordinated engagement of bottom-up and ACC afferents converging onto L1 NGF cells (Fig. 4). We therefore hypothesized that this augmentation should be dependent upon bottom-up sensory activity, and that dampening of sensory signaling would impair this phenomenon. To achieve this, we either injected AAV-DIO-hM4D(Gi)-DREADD-tBFP into the dLGN (in *Vipr2-Cre* pups) or we enucleated the mice at P4, while expressing Gq-DREADD and hChR2 in ACC and similarly performed whole-cell recording at P13-P15 (Fig. 5H–I). Consistent with our hypothesis, both manipulations reversed the ability of Gq-DREADD activation of ACC from increasing the synaptic strength of ACC afferents onto L1 NGF cells (Fig. 5J).

Next, we queried whether there exists a threshold requirement for bottom-up activity or if enhanced co-activation of ACC and dLGN afferents would further increase the strength of the ACC inputs. To explore this question, we injected the dLGN of *Vipr2-Cre* pups (~P1) and the ACC with a HM3D(Gq)-DREADD-mCherry-expressing AAV and as in earlier experiments, co-injected hChR2-eYFP in the ACC (Fig. S7F, left panel). As expected, upon CNO administration the strength of ACC afferents was increased (Fig. S7F, right panel). However, this did not increase the strength of the ACC afferents beyond what we observed when we activated them in the absence of enhanced dLGN activation (Fig. S7G). We concluded that while activity of dLGN is required for the enhancement of ACC connectivity, additional activation of dLGN does not result in further strengthening of ACC afferents.

Discussion

Interneurons in superficial visual cortex have been shown to receive both bottom-up sensory inputs and top-down cortico-cortical afferents from ACC. Despite the prevalence of ACC fibers in L1 of V1, previous studies have not explored the extent to which INs in this layer receive these inputs. Here, we observe that among L1 INs, NGF cells notably receive

both ACC as well as bottom-up sensory afferents. In addition, we demonstrate that a small portion of the dLGN afferents to L1 are shared with those in L4. Furthermore, we find that during development, the strengthening of ACC afferents onto L1 NGF cells requires the earlier receipt of thalamic inputs from the dLGN. In exploring the role of coordinated activity between ACC and thalamic fibers, we find that chemogenetic activation of the ACC can modulate the strength of these top-down inputs. In contrast, while thalamic afferents are necessary for acquisition of ACC inputs to NGF cells, a threshold level of activity was seen to be sufficient.

L1 NGF cells receive early thalamic inputs

In our rabies tracing of L1 INs in V1, we observed that thalamic afferents originate from both dLGN, as well as higher-order LP thalamus. While dLGN is thought to convey primarily sensory signals, the LP receives input from a variety of sources, including the superior colliculus (Gale and Murphy 2014, Fang, Chou et al. 2020) as well as cortical feedback (Bennett, Gale et al. 2019). This suggests that the activity in LP reflects higher order signaling from a variety of modalities in addition to visual inputs. How these two sources of thalamic input are coordinated within L1 INs is poorly understood. Recent work has implicated the LP activity playing a role to suppress noise in the visual cortex through a L1 mechanism (Fang, Chou et al. 2020). However, the specific INs within L1 that mediate this signaling remain unknown. Despite the presence of both first- and higher-order thalamic inputs to NDNF+ L1 INs, our findings indicate that in this layer, these INs are more abundantly innervated by the dLGN. Interestingly, this trend shifts in enucleated mice, where the size of LP and LD inputs become equivalent to those from the dLGN.

Previous work from our laboratory and others have demonstrated that superficial NGF cells receive thalamic inputs at early postnatal ages (De Marco García, Priya et al. 2015, Che, Babij et al. 2018). Despite their positioning in superficial cortex by P15, NGF cells receive bottom-up activity. They perhaps receive these afferents as early as the SST INs in deep layers, the latter of which are the first born IN population (Marques-Smith, Lyngholm et al. 2016, Tuncdemir, Wamsley et al. 2016, Pouchelon 2020). Given that first-order thalamic inputs are present in both L4 and L1 in V1, it is appealing to consider whether the coordinated induction of excitation within L4 and inhibition within L1 may have developmental functional significance. Nonetheless, despite the considerable strength of dLGN inputs onto L1 NGF cells, our preliminary examination of their output during development (results not shown) suggests that these connections may not produce strong inhibition. Instead, our results indicate that the sensory thalamic inputs to L1 NGF cells are essential for the promotion of afferent connectivity from the ACC, perhaps through a coincident depolarization and Hebbian mechanism, increasing both synapse number and strength. Interestingly, previous work from our group indicates that early thalamic inputs to S1 function competitively with local excitatory inputs to NGF cells (De Marco García, Priya et al. 2015). Specifically, when NMDA signaling is ablated, it resulted in a shift in the connectivity of these cells from receiving thalamic to receiving local cortical afferents. Notably, this study focused on L2/3 NGF cells rather than those in L1. Our present work reveals that thalamic afferents onto L1 NGF cells in visual cortex cooperate with long-range inputs from ACC, resulting in their developmental strengthening. Taken together, these

results indicate that local and long-range connectivity onto L1 NGF cells are centrally dependent on early thalamic afferents.

L1 NGF cells function in the coordination of bottom-up and top-down signaling

While L1 INs have been previously shown to receive bottom-up sensory inputs (Ji, Zingg et al. 2015), we demonstrate that this is specific to the NGF cell population during development. In addition, the dLGN afferents to L1 NGF cells at least in part represent efferent copy of the sensory afferents to the L4 cells. This suggests that NGF cells in L1 are uniquely positioned to coordinate the activity of bottom-up and top-down signaling in the superficial layers of the visual cortex. It is likely that thalamic first-order afferents to the NGF cells synergize with projections from other sources. While previous studies implicate that cholinergic afferents may subserve this role (Letzkus, Wolff et al. 2011, Alitto and Dan 2012, Fan, Kheifets et al. 2020), our work implicates the co-recruitment of ACC afferents as a potential source for their engagement.

L1 NGF cells have late-spiking properties and are thought to signal through volume transmission, which provides strong and sustained inhibition in superficial visual cortex. This positions them to function in suppressing activity when bottom-up and top-down signals are coordinated. This could be potentially useful in contexts where the expected internal representation is in concordance with bottom-up sensory signals. They therefore could be functioning in a manner akin to what has been proposed for PV interneurons, which have been implicated in the suppression of self-generated movements in the auditory cortex (Schneider, Sundararajan et al. 2018). In a complementary fashion to the L1 NGF cells, VIP INs in L2/3 also receive top-down signals including from ACC (Zhang, Xu et al. 2014), but notably not direct bottom-up inputs (Ji, Zingg et al. 2015). VIP INs disinhibit SST INs (Lee, Kruglikov et al. 2013, Fu, Tucciarone et al. 2014), the latter of which has been shown to be activated during visual-learning (Attinger, Wang et al. 2017). Our results indicate that the ACC connectivity onto VIP INs is not altered with sensory deprivation, suggesting a role for bottom-up inputs in the strengthening of ACC afferents specifically onto L1 NGF cells. Interestingly, the RSP inputs onto L1 NGF cells were also not significantly altered in enucleated mice. In part, this was expected based on the lack of developmental modulation of these inputs onto L1 NGF cells. But it was also surprising, since it could be expected that navigation-based top-down circuitry requires sensory inputs/experience. Based on our results, it is likely that either these connections are either hardwired and minimally altered across development/sensory manipulations; or that other inputs are more important in the establishment of RSP connectivity.

Thus, emerging evidence has begun to reveal how different IN populations are coordinated to support cortical computations. Our findings provide insight as to the contexts in which L1 NGF cells are likely recruited. Interestingly, we have observed that the NGF cells in the auditory cortex are organized similarly to those we report here (data not shown). Future experiments will reveal how these populations are engaged *in vivo* in both auditory and visual tasks, and how the balance between bottom-up and top-down circuit development is disrupted in neurodevelopmental and neuropsychiatric disorders.

STAR * Methods

RESOURCE AVAILABILITY

Lead Contact—Further information and requests for reagent should be directed to the Lead Contact Gord Fishell (gordon_fishell@hms.harvard.edu)

Materials Availability—Plasmids and viruses created in this study are available upon request from the Lead Contact.

Data and Code Availability

- Microscopy and electrophysiology data reported in this paper will be shared by the lead contact upon request.
- Software used for data analysis are included in the key resources table
- Any additional information required to reanalyze the data reported in this work paper is available from the Lead Contact upon request.

EXPERIMENTAL MODEL AND SUBJECT DETAILS

Mice—All experiments were approved by and in accordance with Harvard Medical School IACUC protocol number IS00001269. C57Bl/6 mice were used for breeding with transgenic mice. Transgenic mice, NDNF-dgCre (Jax stock number: 028536), Vipr2-IRES-Cre-D (stock number: 031332), Scnn1a-Tg3-Cre (Jax stock number: 009613), VIP-IRES-Cre (Jax stock #010908), PV-IRES-Cre (Jax stock #017320), SST-IRES-Cre (Jax stock # #013044), Ai14 (expressing tdTomato, stock number: 007909), Sun1-GFP (Jax stock #021039) are available at Jackson Laboratories. Animals were group housed and maintained under standard, temperature-controlled laboratory conditions. Mice were kept on a 12:12 light/dark cycle and received water and food *ad libitum*. For experiments during development, mice were injected at ~P1 and experiments conducted between ages P13-P15. In the case of adults, mice were injected at P30, and experiments conducted between ages P45-P50. Both female and male were used in the entire study and similar results were obtained in both sexes.

METHOD DETAILS

Sensory deprivations—To deprive mice from visual sensory input enucleation was performed. P4 mouse pups were anesthetized by hypothermia. A small incision was made between the eyelids with a scalpel and the eye was separated from the optic nerve with micro-scissors to be removed from the orbit. The incision was secured using biocompatible Vetbond glue. The pups were then allowed to recover on a heating pad before being returned to their mother. Dark rearing was performed by putting the cage (mom with P4 pups) in a tightly dark chamber, where temperature and humidity were controlled. Mice were monitored on a daily basis (in the dark) to make sure they have adequate food and water.

Histology—Mice at between P42-P46 for the adult time point or P15 for the developmental time point were transcardially perfused with 4% paraformaldehyde (PFA) and brains were fixed overnight in 4% PFA at 4 °C. 50μm vibratome sections were used

for all histological experiments. Every 3rd representative section was collected, and the sections were processed for immunohistochemistry. For immunofluorescence, brain sections were incubated for 1 h at room temperature in a blocking solution containing 10% normal donkey serum (NDS) and 0.3% triton X-100 in PBS and incubated overnight at 4°C with primary antibodies: goat anti-mCherry (1:1,000; SicGen), chicken anti-GFP (1:1000; Aves Labs #1020) and/or mouseIgG2A anti-ChR2 (1:200; ARP Inc). Sections were rinsed three times in PBS and incubated for 60–90 min at room temperature or overnight at 4°C with the Alexa Fluor 488- and 594- and 647-conjugated secondary antibodies (1:500; Thermo Fisher Science or Jackson ImmunoResearch).

For L1 IN morphology, cells filled with biocytin were stained with Streptavidin-conjugated with Alexa 647. Briefly, recorded sections were postfixed with 4% PFA overnight, rinsed in PBS, cleared in Cubic1 solution (as described in (Schuman, Machold et al. 2018, Schuman, Machold et al. 2019), blocked with Normal Donkey Serum and stained with Streptavidin-647 (1:500, ThermoFisher Scientific Cat # S32357) and anti-GFP (to visualize ACC fibers). The sections were then washed, cleared in Cubic2 solution and mounted for confocal imaging using Zeiss LSM 800 microscope.

Rabies tracing—For tracing afferents from NDNF+ neurons in V1, stereotactic injections were performed between P30-P35 in the case of adult mice. AAV-helpers (Titer of 9.5×10^{12} vg/mL) and N2c-RV-mCherry were diluted with PBS at a ratio of 1:1 and 50nL was injected using NanojectIII at 1nL/s in V1 (AP-3.5mm, ML-2.5mm, DV-0.20mm). Animals were perfused 14 days later. For developmental time points, stereotaxic injections were performed using a neonate adapter (Harvard apparatus). Mouse pups were anesthetized by hypothermia and stereotaxically injected with the viruses at P1 (From Lambda: AP+0.2mm, ML-1.60mm, DV-0.1mm). Animals were perfused 14 days later at P15. All coordinates were determined to target mainly L1 of the cortex. In the case of RV tracing from L4 neurons, AAV helper and RV were injected at a depth of DV-0.5mm.

Viruses

For rabies tracing: AAV2/1-DIO-helper virus encoding N2c-G-P2A-TVA-P2A-eGFP (NYUAD and designed from VTKS2 backbone Addgene #170853) was expressed in a single AAV vector as described in (Pouchelon 2020). EnvA-pseudotyped CVS-N2c(ΔG)-FlpO-mCherry was used. The RV CVS-N2c(DG)-mCherry-P2A-FlpO was a gift from Thomas Jessell (Addgene plasmid # 73471; (Reardon, Murray et al. 2016) and the N2c-RV were either produced, amplified and EnvA-pseudotyped in the lab, or generously shared by K. Ritola at Janelia Farms Research Center.

Other viruses used in the paper: AAV2/1-hSyn-hChR2(H134R)-EYFP was a gift from Karl Deisseroth (Addgene #26973-AAV1; (Boyden, Zhang et al. 2005); AAV2/1-hSyn-hM3D(Gq)-mCherry was a gift from Bryan Roth (Addgene #50474-AAV2; (Krashes, Koda et al. 2011); AAV(PHP-eb)-hSyn-DIO-hM3D(Gq)-mCherry was a gift from Bryan Roth (Addgene #44361-PHP-eB); AAV2/1-Ef1a-fDIO-hChr2-eYFP was a gift from Karl Deisseroth (Addgene #55639-AAV1; (Fenno, Mattis et al. 2014); pAAV2/1-EF1a-DIO-hChR2-eYFP/mCherry was a gift from Karl Deisseroth (Addgene #20298/20297-AAV1);

AAV2/1-hSyn-fDIO-DTA (NYUAD, designed from VTKS3 backbone, Addgene #170854); AAV2/1-hSyn-DIO-hM4D(Gi)-tagBFP (NYUAD, designed from VTKS2 backbone, Addgene #170853). pENN-AAV2/1-CamKII-Cre.SV40 was a gift from James Wilson (Addgene #105558). AAV (PHP-eb)-S5E2-GFP was a gift from Jordane Dimidschtein (Addgene #135631; (Vormstein-Schneider, Lin et al. 2020).

Trans-synaptic labeling

Retina Injections: 1.5 μl pENN-AAV2/1-CamKII-Cre.SV40 (Titer of 1×10^{13} vg/mL) was injected in the right retina (750nL in dorsal and 750nL in ventral retina).

dLGN injections: 700nL of pAAV2/1-EF1a-DIO-hChR2-mCherry (Titer of 5×10^{12} vg/mL) was injected into the contralateral dLGN at different depth spread over 3 different depths to cover the dLGN (2.2mm, −2.3mm, 2.5−2.75mm).

Imaging analysis—Each brain section containing labelled cells was acquired as a tiled image on a motorized tiling scope Zeiss Axio Imager A1. Starter cells (colocalization of GFP^+ AAV-helpers and $mCherry^+$ RV) were manually quantified on ImageJ software. Brains with more than 10 non-L1 starter cells were not included in the analysis. $mCherry^+$ retrogradely labeled cells were registered for each region of the Allen Reference Brain atlas for adult brain and of the “Atlas of Developing Mouse Brain at P6” from George Paxinos 2006. The number of retrogradely labeled cells in a given region were normalized to the total number of cells labeled in the entire brain for the analysis in Fig. 1E; to the total number of retrogradely labeled cells within V1 (Fig. S1A–B) or to the total number of retrogradely labeled cells in the visual thalamus (Fig. S1C–D).

Stereotaxic Injections for optogenetics and slice recording

For ACC injections: 80nL of 1:1 dilution (with PBS) of AAV1-hSyn-hChR2(H134R)-eYFP (Titer of 1×10^{13} vg/mL) was injected in the left ACC using the following coordinates for adult [AP 0.5mm, ML 0.35mm, DV 0.5mm], and for development (50nL 1:1 dilution [From Lambda: AP 2mm, ML 0.2mm, DV 0.5mm].

For RSP injections, the following coordinates were used for developmental time point [From Lambda: AP 1.4mm, ML 0.2mm, DV 0.5mm] and for adults [AP −2mm, ML 0.5mm, DV 0.5mm].

For dLGN injections: 50nL AAV1-EF1a-DIO-hChR2(H134R)-eYFP was injected in the left dLGN of Vipr2-IRES-Cre-D mice using stereotaxic injection at P1 for developmental time point [From Lambda: AP 0.8mm, ML 1.3mM, DV 1.4mm]. Either WT mice injected with AAV1-hSyn-hChR2(H134R)-eYFP (100nl 5×10^{12} vg/mL) or Vipr2-IRES-Cre-D mice were injected with AAV1-EF1a-DIO-hChR2(H134R)-eYFP (100nL 5×10^{12} vg/mL) at ~P30–35 for the adult time point [AP −2.3mm, ML 2.2mm, DV 2.6mm].

Animal selection criteria: Mice with non-uniform or non-specific injections in either ACC or dLGN were excluded from the study.

In the case of PV INs recording, either PV-Cre::Sun1-GFP mice were used; or PV neurons were labeled using an AAV with a PV-specific enhancer (S5E2; (Vormstein-Schneider, Lin et al. 2020)

In vitro electrophysiology—P13-P15 were decapitated, and the brain was quickly removed and immersed in ice-cold oxygenated (95% O2 / 5% CO2) sucrose cutting solution containing 87 mM NaCl, 2.5 mM KCl, 2 mM $MgCl_2$, 1 mM $CaCl_2$, 1.25 mM NaH_2PO_4, 26 mM $NaHCO_3$, 10 mM glucose and 75 mM sucrose (pH 7.4). 300μm thick coronal slices were cut using a Leica VT 1200S vibratome through V1. Slices were recovered in a holding chamber with artificial cerebrospinal fluid (aCSF) containing 124 mM NaCl, 20 mM Glucose, 3 mM KCl, 1.2 mM NaH_2PO_4, 26 mM $NaHCO_3$, 2 mM $CaCl_2$, 1 mM $MgCl_2$ (pH 7.4) at 34 °C for 30 minutes and at room temperate for at least 45 minutes prior to recordings. For adult recordings, mice were perfused with NMDG cutting solution containing 92mM NMDG, 2.5mM KCl, 1.2mM NaH_2PO_4, 30mM $NaHCO_3$, 20mM HEPES, 25mM glucose, 5mM sodium ascorbate, 3mM sodium pyruvate, 0.5mM $CaCl_2$, 10mM $MgSO_4$. During recovery, the NaCl was gradually added as described in (Ting, Lee et al. 2018). For recordings, slices were transferred to an upright microscope (Zeiss) with IR-DIC optics. Cells were visualized using a 40x water immersion objective. Slices were perfused with aCSF in a recording chamber at 2 mL/min at 30C. All slice preparation and recording solutions were oxygenated with carbogen gas (95% O_2, 5% CO_2, pH 7.4). Patch electrodes (3–6 MΩ) were pulled from borosilicate glass (1.5 mm OD, Harvard Apparatus). For all recordings patch pipettes were filled with an internal solution containing: 125 mM Cs-gluconate, 2 mM CsCl, 10 mM HEPES, 1 mM EGTA, 4 mM MgATP, 0.3 mM NaGTP, 8 mM Phosphocreatine-Tris, 1 mM QX-314-Cl, equilibrated with CsOH at pH 7.3 or 130 K-Gluconate, 10 KCl, 10 HEPES, 0.2 EGTA, 4 MgATP, 0.3 NaGTP, 5 Phosphocreatine and 0.4% biocytin, equilibrated with KOH CO2 to a pH=7.3.

Recordings were performed using a Multiclamp 700B amplifier (Molecular Devices) and digitized using a Digidata 1440A and the Clampex 10 program suite (Molecular Devices). Voltage-clamp signals were filtered at 3 kHz and recorded with a sampling rate of 10 kHz. Recordings were performed at a holding potential of −70 mV. Cells were only accepted for analysis if the initial series resistance was less than 40 MΩ and did not change by more than 20% during the recording period. The series resistance was compensated at least ~30% in voltage-clamp mode and no correction were made for the liquid junction potential. Whole-cell patch-clamp recordings were obtained from L1 INs and pyramidal-shaped neurons in L2/3 or L4 located in the same column. To activate afferents expressing hChR2, blue light was transmitted from a collimated LED (Mightex) attached to the epifluorescence port of the upright microscope. 5ms or 1ms pulses of a fixed light intensity were directed to the slice in the recording chamber via a mirror coupled to the 40x objective. Flashes were delivered every 15 s for a total of 10 trials. The LED output was driven by a transistor-transistor logic output from the Clampex software. In some cases, recordings were performed in the presence of 1 μm TTX and 1 mM 4-AP (Tocris) (after identifying cell type without drugs) to reveal pure monosynaptic inputs. We only used cells that were monosynaptic based on latency of the response, which was found to be 3ms on average from the start of the light stimulation.

None of the experiments were blinded to the conditions. In some cases, a different experimenter confirmed the findings.

Data Analysis: Passive and active membrane properties were recorded in current clamp mode by applying a series of hyperpolarizing and depolarizing current steps. All intrinsic physiological properties were analyzed using Clampfit10.7 and Easy Electrophysiology V2.2. The Resting membrane potential was recorded soon after break-in at I=0. The cell input resistance was calculated from the peak of the voltage response to a 200pA hyperpolarizing 1-second-long current step according to Ohm's law. The sag or hump peak voltage deflection is calculated as the difference between peak membrane potential and baseline based on a 200pA hyperpolarizing current injection. Analysis of the action potential properties was done on the first spike observed during a series of depolarizing steps. Threshold was defined as the voltage at the point when the slope first exceeds a value of 20 Vs^{-1}. Rheobase was defined as the amplitude of the first depolarizing current step at which firing was observed. Spike half width is defined as the width at half amplitude. Fast hyperpolarization (fAHP) is calculated as the difference between spike threshold and minimum the voltage after the spike within 3ms. mAHP is defined as difference between spike threshold and minimum voltage after the spike, from 10 to 50ms. Analysis of spontaneous inhibitory events was done using Clampfit's threshold search. For optogenetic experiments, data analysis was performed off-line using the Clampfit 10.7 module of pClamp (Molecular Devices) and Prism 8 (GraphPad). The amplitude of evoked synaptic currents to 5ms blue-light stimulation was obtained by averaging the peak amplitude of individual waveforms over 10 trials per cell. EPSC amplitudes recorded from L1 INs were then normalized for injection size by dividing the average EPSC by the evoked current amplitude from a putative L2/3 or L4 pyramidal neuron in the same column of each slice. Failure rate was computed as the percentage of trials that evoked no response of any amplitude in response to a 1ms blue-light stimulation.

CNO injections—CNO (diluted in DMSO and saline, Tocris Cat #4936) was injected at a concentration of 0.01mg/kg of body weight and was injected daily starting at either P5 or P11, until recording day (P13-P15). Injections were made in the milk sac of the pups, and later injections were made intraperitoneally.

Neurolucida tracing—Sections containing the axons of interest were imaged on a Zeiss LSM 800. Z-stacks of images were then loaded into Neurolucida 360 (MBF Biosciences) and trees were reconstructed using the 'user guided' option with Directional Kernels.

Quantification and Statistical Analysis—No prior test for determining sample size was conducted. All statistical analyses were performed using Prism (GraphPad). Statistical significance was tested with non-paired, two-sided t-test, with a 95% confidence interval or One-Way ANOVA with Tukey's correction for multiple comparisons. In some cases, One-Way ANOVA with Brown-Forsythe test was used in the cases where SD was not equal. All data are presented as mean ± SEM unless otherwise stated. Across the manuscript, N refers to number of animals, whereas n refers to number of cells. This information is included in the legends for each figure.

Supplementary Material

Refer to Web version on PubMed Central for supplementary material.

ACKNOWLEDGEMENTS

We thank Dr. Anne Takesian and Dr. Chinfei Chen for their valuable comments on the manuscript. We also thank Dr. Gabrielle Pouchelon and Dr. Shruti Muralidhar for proof-reading the manuscript. We thank Dr. Tim Burbridge for demonstrating retinal injections. This work was supported by a Goldenson Foundation (FY18) and a Hearst foundation grant (FY19) (to LAI) and by grants from the National Institutes of Health (NIH): MH071679, NS08297, NS074972, MH095147 to GF and grants P01NS074972, R01NS107257, and R01NS110079 to BR, as well as support from the Simons Foundation (SFARI) (to G.F).

References

Abs E, Poorthuis RB, Apelblat D, Muhammad K, Pardi MB, Enke L, Kushinsky D, Pu DL, Eizinger MF, Conzelmann KK, Spiegel I. and Letzkus JJ (2018). “Learning-Related Plasticity in DendriteTargeting Layer 1 Interneurons.” Neuron 100(3): 684–699.e686. [PubMed: 30269988]

Alitto HJ and Dan Y. (2012). “Cell-type-specific modulation of neocortical activity by basal forebrain input.” Front Syst Neurosci 6: 79. [PubMed: 23316142]

Anastasiades PG, Collins DP and Carter AG (2020). “Mediodorsal and Ventromedial Thalamus Engage Distinct L1 Circuits in the Prefrontal Cortex.” Neuron.

Ardid S, Wang XJ and Compte A. (2007). “An integrated microcircuit model of attentional processing in the neocortex.” J Neurosci 27(32): 8486–8495. [PubMed: 17687026]

Attinger A, Wang B. and Keller GB (2017). “Visuomotor Coupling Shapes the Functional Development of Mouse Visual Cortex.” Cell 169(7): 1291–1302.e1214. [PubMed: 28602353]

Bennett C, Gale SD, Garrett ME, Newton ML, Callaway EM, Murphy GJ and Olsen SR (2019). “Higher-Order Thalamic Circuits Channel Parallel Streams of Visual Information in Mice.” Neuron 102(2): 477–492.e475. [PubMed: 30850257]

Bhandari A. (2020). Bilateral enucleation induces homeostatic plasticity in the dorsolateral geniculate nucleus of mice.

Boyden ES, Zhang F, Bamberg E, Nagel G. and Deisseroth K. (2005). “Millisecond-timescale, genetically targeted optical control of neural activity.” Nat Neurosci 8(9): 1263–1268. [PubMed: 16116447]

Che A., Babij R, Iannone AF, Fetcho RN, Ferrer M, Liston C, Fishell G and De Marco García NV (2018). “Layer I Interneurons Sharpen Sensory Maps during Neonatal Development.” Neuron 99(1): 98116.e117.

Chou SJ, Babot Z, Leingärtner A, Studer M, Nakagawa Y. and O’Leary DD (2013). “Geniculocortical input drives genetic distinctions between primary and higher-order visual areas.” Science 340(6137): 1239–1242. [PubMed: 23744949]

Cohen-Kashi Malina K, Tsivourakis E, Kushinsky D, Apelblat D, Shtiglitz S, Zohar E, Sokoletsky M, Tasaka GI, Mizrahi A, Lampl I. and Spiegel I. (2021). “NDNF interneurons in layer 1 gain-modulate whole cortical columns according to an animal’s behavioral state.” Neuron.

Colonnese MT, Kaminska A, Minlebaev M, Milh M, Bloem B, Lescure S, Moriette G, Chiron C, Ben-Ari Y. and Khazipov R. (2010). “A conserved switch in sensory processing prepares developing neocortex for vision.” Neuron 67(3): 480–498. [PubMed: 20696384]

Cruikshank SJ, Ahmed OJ, Stevens TR, Patrick SL, Gonzalez AN, Elmaleh M. and Connors BW (2012). “Thalamic control of layer 1 circuits in prefrontal cortex.” J Neurosci 32(49): 17813–17823. [PubMed: 23223300]

De Marco García NV, Priya R, Tuncdemir SN, Fishell G. and Karayannis T. (2015). “Sensory inputs control the integration of neurogliaform interneurons into cortical circuits.” Nat Neurosci 18(3): 393–401. [PubMed: 25664912]

Desimone R. and Duncan J. (1995). “Neural mechanisms of selective visual attention.” Annu Rev Neurosci 18: 193–222. [PubMed: 7605061]

Dominguez S, Ma L, Yu H, Pouchelon G, Mayer C, Spyropoulos GD, Cea C, Buzsáki G, Fishell G, Khodagholy D. and Gelinas JN (2021). “A transient postnatal quiescent period precedes emergence of mature cortical dynamics.” Elife 10.

Fan LZ, Kheifets S, Böhm UL, Wu H, Piatkevich KD, Xie ME, Parot V, Ha Y, Evans KE, Boyden ES, Takesian AE and Cohen AE (2020). “All-Optical Electrophysiology Reveals the Role of Lateral Inhibition in Sensory Processing in Cortical Layer 1.” Cell 180(3): 521–535.e518. [PubMed: 31978320]

Fang Q, Chou XL, Peng B, Zhong W, Zhang LI and Tao HW (2020). “A Differential Circuit via Retino-Colliculo-Pulvinar Pathway Enhances Feature Selectivity in Visual Cortex through Surround Suppression.” Neuron 105(2): 355–369.e356. [PubMed: 31812514]

Fenno LE, Mattis J, Ramakrishnan C, Hyun M, Lee SY, He M, Tucciarone J, Selimbeyoglu A, Berndt A, Grosenick L, Zalocusky KA, Bernstein H, Swanson H, Perry C, Diester I, Boyce FM, Bass CE, Neve R, Huang ZJ and Deisseroth K. (2014). “Targeting cells with single vectors using multiple-feature Boolean logic.” Nat Methods 11(7): 763–772. [PubMed: 24908100]

Fischer LF, Mojica Soto-Albors R, Buck F. and Harnett MT (2020). “Representation of visual landmarks in retrosplenial cortex.” Elife 9.

Frangeul L, Kehayas V, Sanchez-Mut JV, Fièvre S, Krishna-K K, Pouchelon G, Telley L, Bellone C, Holtmaat A, Gräff J, Macklis JD and Jabaudon D. (2017). “Input-dependent regulation of excitability controls dendritic maturation in somatosensory thalamocortical neurons.” Nat Commun 8(1): 2015.

Fu Y, Tucciarone JM, Espinosa JS, Sheng N, Darcy DP, Nicoll RA, Huang ZJ and Stryker MP (2014). “A cortical circuit for gain control by behavioral state.” Cell 156(6): 1139–1152. [PubMed: 24630718]

Gale SD and Murphy GJ (2014). “Distinct representation and distribution of visual information by specific cell types in mouse superficial superior colliculus.” J Neurosci 34(40): 13458–13471. [PubMed: 25274823]

Hooks BM and Chen C. (2020). “Circuitry Underlying Experience-Dependent Plasticity in the Mouse Visual System.” Neuron 106(1): 21–36. [PubMed: 32272065]

Huda R, Sipe GO, Breton-Provencher V, Cruz KG, Pho GN, Adam E, Gunter LM, Sullins A, Wickersham IR and Sur M. (2020). “Distinct prefrontal top-down circuits differentially modulate sensorimotor behavior.” Nat Commun 11(1): 6007. [PubMed: 33243980]

Ibrahim LA, Mesik L, Ji XY, Fang Q, Li HF, Li YT, Zingg B, Zhang LI and Tao HW (2016). “CrossModality Sharpening of Visual Cortical Processing through Layer-1-Mediated Inhibition and Disinhibition.” Neuron 89(5): 1031–1045. [PubMed: 26898778]

Ibrahim LA, Schuman B, Bandler R, Rudy B. and Fishell G. (2020). “Mining the jewels of the cortex’s crowning mystery.” Curr Opin Neurobiol 63: 154–161. [PubMed: 32480351]

Jaepel J., Hübener M, Bonhoeffer T and Rose T (2017). “Lateral geniculate neurons projecting to primary visual cortex show ocular dominance plasticity in adult mice.” Nat Neurosci 20(12): 1708–1714. [PubMed: 29184207]

Ji XY, Zingg B, Mesik L, Xiao Z, Zhang LI and Tao HW (2015). “Thalamocortical Innervation Pattern in Mouse Auditory and Visual Cortex: Laminar and Cell-Type Specificity.” Cereb Cortex.

Jiang X, Wang G, Lee AJ, Stornetta RL and Zhu JJ (2013). “The organization of two new cortical interneuronal circuits.” Nat Neurosci 16(2): 210–218. [PubMed: 23313910]

Kastner S. and Ungerleider LG (2000). “Mechanisms of visual attention in the human cortex.” Annu Rev Neurosci 23: 315–341. [PubMed: 10845067]

Kawaguchi Y. and Kubota Y. (1997). “GABAergic cell subtypes and their synaptic connections in rat frontal cortex.” Cereb Cortex 7(6): 476–486. [PubMed: 9276173]

Krashes MJ, Koda S, Ye C, Rogan SC, Adams AC, Cusher DS, Maratos-Flier E, Roth BL and Lowell BB (2011). “Rapid, reversible activation of AgRP neurons drives feeding behavior in mice.” J Clin Invest 121(4): 1424–1428. [PubMed: 21364278]

Lee AJ, Wang G, Jiang X, Johnson SM, Hoang ET, Lanté F, Stornetta RL, Beenhakker MP, Shen Y. and Julius Zhu J. (2015). “Canonical Organization of Layer 1 Neuron-Led Cortical Inhibitory and Disinhibitory Interneuronal Circuits.” Cereb Cortex 25(8): 2114–2126. [PubMed: 24554728]

Lee S, Kruglikov I, Huang ZJ, Fishell G. and Rudy B. (2013). “A disinhibitory circuit mediates motor integration in the somatosensory cortex.” Nat Neurosci 16(11): 1662–1670. [PubMed: 24097044]

Leinweber M, Ward DR, Sobczak JM, Attinger A. and Keller GB (2017). “A Sensorimotor Circuit in Mouse Cortex for Visual Flow Predictions.” Neuron 96(5): 1204.

Letzkus JJ, Wolff SB, Meyer EM, Tovote P, Courtin J, Herry C. and Lüthi A. (2011). “A disinhibitory microcircuit for associative fear learning in the auditory cortex.” Nature 480(7377): 331–335. [PubMed: 22158104]

Luhmann HJ and Khazipov R. (2018). “Neuronal activity patterns in the developing barrel cortex.” Neuroscience 368: 256–267. [PubMed: 28528963]

Ma G, Liu Y, Wang L, Xiao Z, Song K, Wang Y, Peng W, Liu X, Wang Z, Jin S, Tao Z, Li CT, Xu T, Xu F, Xu M. and Zhang S. (2021). “Hierarchy in sensory processing reflected by innervation balance on cortical interneurons.” Sci Adv 7(20).

Makino H. and Komiyama T. (2015). “Learning enhances the relative impact of top-down processing in the visual cortex.” Nat Neurosci 18(8): 1116–1122. [PubMed: 26167904]

Mao D, Molina LA, Bonin V. and McNaughton BL (2020). “Vision and Locomotion Combine to Drive Path Integration Sequences in Mouse Retrosplenial Cortex.” Curr Biol 30(9): 1680–1688.e1684. [PubMed: 32197086]

Marques-Smith A, Lyngholm D, Kaufmann AK, Stacey JA, Hoerder-Suabedissen A, Becker EB, Wilson MC, Molnár Z. and Butt SJ (2016). “A Transient Translaminar GABAergic Interneuron Circuit Connects Thalamocortical Recipient Layers in Neonatal Somatosensory Cortex.” Neuron 89(3): 536–549. [PubMed: 26844833]

Meng X. (2020). Transient coupling between subplate and subgranular layers to L1 neurons before and during the critical period. Y. Xu and J. P. Y. Kao. BioRxiv.

Mesik L, Huang JJ, Zhang LI and Tao HW (2019). “Sensory and motor-related responses of layer 1 neurons in the mouse visual cortex.” J Neurosci.

Muralidhar S, Wang Y. and Markram H. (2013). “Synaptic and cellular organization of layer 1 of the developing rat somatosensory cortex.” Front Neuroanat 7: 52. [PubMed: 24474905]

Nahmani M. and Turrigiano GG (2014). “Deprivation-induced strengthening of presynaptic and postsynaptic inhibitory transmission in layer 4 of visual cortex during the critical period.” J Neurosci 34(7): 2571–2582. [PubMed: 24523547]

Naskar S., Qi J, Pereira F, Gerfen CR and Lee S (2021). “Cell-type-specific recruitment of GABAergic interneurons in the primary somatosensory cortex by long-range inputs.” Cell Rep 34(8): 108774.

Nassi JJ. and Callaway EM (2009). “Parallel processing strategies of the primate visual system.” Nat Rev Neurosci 10(5): 360–372. [PubMed: 19352403]

Oh SW, Harris JA, Ng L, Winslow B, Cain N, Mihalas S, Wang Q, Lau C, Kuan L, Henry AM, Mortrud MT, Ouellette B, Nguyen TN, Sorensen SA, Slaughterbeck CR, Wakeman W, Li Y, Feng D, Ho A, Nicholas E, Hirokawa KE, Bohn P, Joines KM, Peng H, Hawrylycz MJ, Phillips JW, Hohmann JG, Wohnoutka P, Gerfen CR, Koch C, Bernard A, Dang C, Jones AR and Zeng H. (2014). “A mesoscale connectome of the mouse brain.” Nature 508(7495): 207–214. [PubMed: 24695228]

Palmer LM, Schulz JM, Murphy SC, Ledergerber D, Murayama M. and Larkum ME (2012). “The cellular basis of GABA(B)-mediated interhemispheric inhibition.” Science 335(6071): 989–993. [PubMed: 22363012]

Pardi MB, Vogenstahl J, Dalmay T, Spanò T, Pu DL, Naumann LB, Kretschmer F, Sprekeler H. and Letzkus JJ (2020). “A thalamocortical top-down circuit for associative memory.” Science 370(6518): 844–848. [PubMed: 33184213]

Pouchelon G. (2020). The organization and developmental establishment of cortical interneuron presynaptic circuits. Y. Bollmann. Bioarxiv.

Pouchelon G, Gambino F, Bellone C, Telley L, Vitali I, Lüscher C, Holtmaat A. and Jabaudon D. (2014). “Modality-specific thalamocortical inputs instruct the identity of postsynaptic L4 neurons.” Nature 511(7510): 471–474. [PubMed: 24828045]

Rao RP and Ballard DH (1999). “Predictive coding in the visual cortex: a functional interpretation of some extra-classical receptive-field effects.” Nat Neurosci 2(1): 79–87. [PubMed: 10195184]

Reardon TR, Murray AJ, Turi GF, Wirblich C, Croce KR, Schnell MJ, Jessell TM and Losonczy A. (2016). “Rabies Virus CVS-N2c(ΔG) Strain Enhances Retrograde Synaptic Transfer and Neuronal Viability.” Neuron 89(4): 711–724. [PubMed: 26804990]

Rose T, Jaepel J, Hübener M. and Bonhoeffer T. (2016). “Cell-specific restoration of stimulus preference after monocular deprivation in the visual cortex.” Science 352(6291): 1319–1322. [PubMed: 27284193]

Roth MM, Dahmen JC, Muir DR, Imhof F, Martini FJ and Hofer SB (2016). “Thalamic nuclei convey diverse contextual information to layer 1 of visual cortex.” Nat Neurosci 19(2): 299–307. [PubMed: 26691828]

Saalmann YB, Pinsk MA, Wang L, Li X. and Kastner S. (2012). “The pulvinar regulates information transmission between cortical areas based on attention demands.” Science 337(6095): 753–756. [PubMed: 22879517]

Schneider DM, Sundararajan J. and Mooney R. (2018). “A cortical filter that learns to suppress the acoustic consequences of movement.” Nature 561(7723): 391–395. [PubMed: 30209396]

Schuman B, Dellal S, Prönneke A, Machold R. and Rudy B. (2021). “Neocortical Layer 1: An Elegant Solution to Top-Down and Bottom-Up Integration.” Annu Rev Neurosci.

Schuman B, Machold R, Hashikawa Y, Fuzik J, Fishell G. and Rudy B. (2018). “Four unique interneuron populations reside in neocortical layer 1.” J Neurosci.

Schuman B, Machold RP, Hashikawa Y, Fuzik J, Fishell GJ and Rudy B. (2019). “Four Unique Interneuron Populations Reside in Neocortical Layer 1.” J Neurosci 39(1): 125–139. [PubMed: 30413647]

Squire RF, Noudoost B, Schafer RJ and Moore T. (2013). “Prefrontal contributions to visual selective attention.” Annu Rev Neurosci 36: 451–466. [PubMed: 23841841]

Takesian AE, Bogart LJ, Lichtman JW and Hensch TK (2018). “Inhibitory circuit gating of auditory critical-period plasticity.” Nat Neurosci 21(2): 218–227. [PubMed: 29358666]

Tasic B, Menon V, Nguyen TN, Kim TK, Jarsky T, Yao Z, Levi B, Gray LT, Sorensen SA, Dolbeare T, Bertagnolli D, Goldy J, Shapovalova N, Parry S, Lee C, Smith K, Bernard A, Madisen L, Sunkin SM, Hawrylycz M, Koch C. and Zeng H. (2016). “Adult mouse cortical cell taxonomy revealed by single cell transcriptomics.” Nat Neurosci 19(2): 335–346. [PubMed: 26727548]

Tasic B., Yao Z, Graybuck LT, Smith KA, Nguyen TN, Bertagnolli D, Goldy J, Garren E, Economo MN, Viswanathan S, Penn O, Bakken T, Menon V, Miller J, Fong O, Hirokawa KE, Lathia K, Rimorin C, Tieu M, Larsen R, Casper T, Barkan E, Kroll M, Parry S, Shapovalova NV, Hirschstein D, Pendergraft J, Sullivan HA, Kim TK, Szafer A, Dee N, Groblewski P, Wickersham I, Cetin A, Harris JA, Levi BP, Sunkin SM, Madisen L, Daigle TL, Looger L, Bernard A, Phillips J, Lein E, Hawrylycz M, Svoboda K, Jones AR, Koch C and Zeng H (2018). “Shared and distinct transcriptomic cell types across neocortical areas.” Nature 563(7729): 72–78. [PubMed: 30382198]

Ting JT, Lee BR, Chong P, Soler-Llavina G, Cobbs C, Koch C, Zeng H. and Lein E. (2018). “Preparation of Acute Brain Slices Using an Optimized N-Methyl-D-glucamine Protective Recovery Method.” J Vis Exp(132).

Tuncdemir SN, Wamsley B, Stam FJ, Osakada F, Goulding M, Callaway EM, Rudy B. and Fishell G. (2016). “Early Somatostatin Interneuron Connectivity Mediates the Maturation of Deep Layer Cortical Circuits.” Neuron 89(3): 521–535. [PubMed: 26844832]

Vormstein-Schneider D, Lin JD, Pelkey KA, Chittajallu R, Guo B, Arias-Garcia MA, Allaway K, Sakopoulos S, Schneider G, Stevenson O, Vergara J, Sharma J, Zhang Q, Franken TP, Smith J, Ibrahim LA, M Astro KJ, Sabri E, Huang S, Favuzzi E, Burbridge T, Xu Q, Guo L, Vogel I, Sanchez V, Saldi GA, Gorissen BL, Yuan X, Zaghloul KA, Devinsky O, Sabatini BL, Batista-Brito R, Reynolds J, Feng G, Fu Z, McBain CJ, Fishell G. and Dimidschstein J. (2020). “Viral manipulation of functionally distinct interneurons in mice, non-human primates and humans.” Nat Neurosci 23(12): 1629–1636. [PubMed: 32807948]

Wickersham IR, Lyon DC, Barnard RJ, Mori T, Finke S, Conzelmann KK, Young JA and Callaway EM (2007). “Monosynaptic restriction of transsynaptic tracing from single, genetically targeted neurons.” Neuron 53(5): 639–647. [PubMed: 17329205]

Williams AL, Reese BE and Jeffery G. (2002). “Role of retinal afferents in regulating growth and shape of the lateral geniculate nucleus.” J Comp Neurol 445(3): 269–277. [PubMed: 11920706]

Zhang S, Xu M, Kamigaki T, Hoang Do JP, Chang WC, Jenvay S, Miyamichi K, Luo L. and Dan Y. (2014). “Selective attention. Long-range and local circuits for top-down modulation of visual cortex processing.” Science 345(6197): 660–665. [PubMed: 25104383]

Zhu Y. and Zhu JJ (2004). “Rapid arrival and integration of ascending sensory information in layer 1 nonpyramidal neurons and tuft dendrites of layer 5 pyramidal neurons of the neocortex.” J Neurosci 24(6): 1272–1279. [PubMed: 14960597]

Zhuang J. (2019). The spatial structure of feedforward information in mouse primary visual cortex. R. S. Larsen. BioRxiv.

Zingg B, Chou XL, Zhang ZG, Mesik L, Liang F, Tao HW and Zhang LI (2017). “AAV-Mediated Anterograde Transsynaptic Tagging: Mapping Corticocollicular Input-Defined Neural Pathways for Defense Behaviors.” Neuron 93(1): 33–47. [PubMed: 27989459]

Zingg B, Hintiryan H, Gou L, Song MY, Bay M, Bienkowski MS, Foster NN, Yamashita S, Bowman I, Toga AW and Dong HW (2014). “Neural networks of the mouse neocortex.” Cell 156(5): 1096–1111. [PubMed: 24581503]

Highlights

- During development L1 NGF cells receive strong dLGN inputs but weak ACC connectivity.
- ACC inputs onto L1 NGF cells, but not onto ‘Canopy’ cells, strengthens in the adult.
- Sensory deprivation blocked the strengthening of ACC afferents onto L1 NGF cells.
- Early ACC is precociously strengthened by stimulation, in a thalamic-dependent manner.

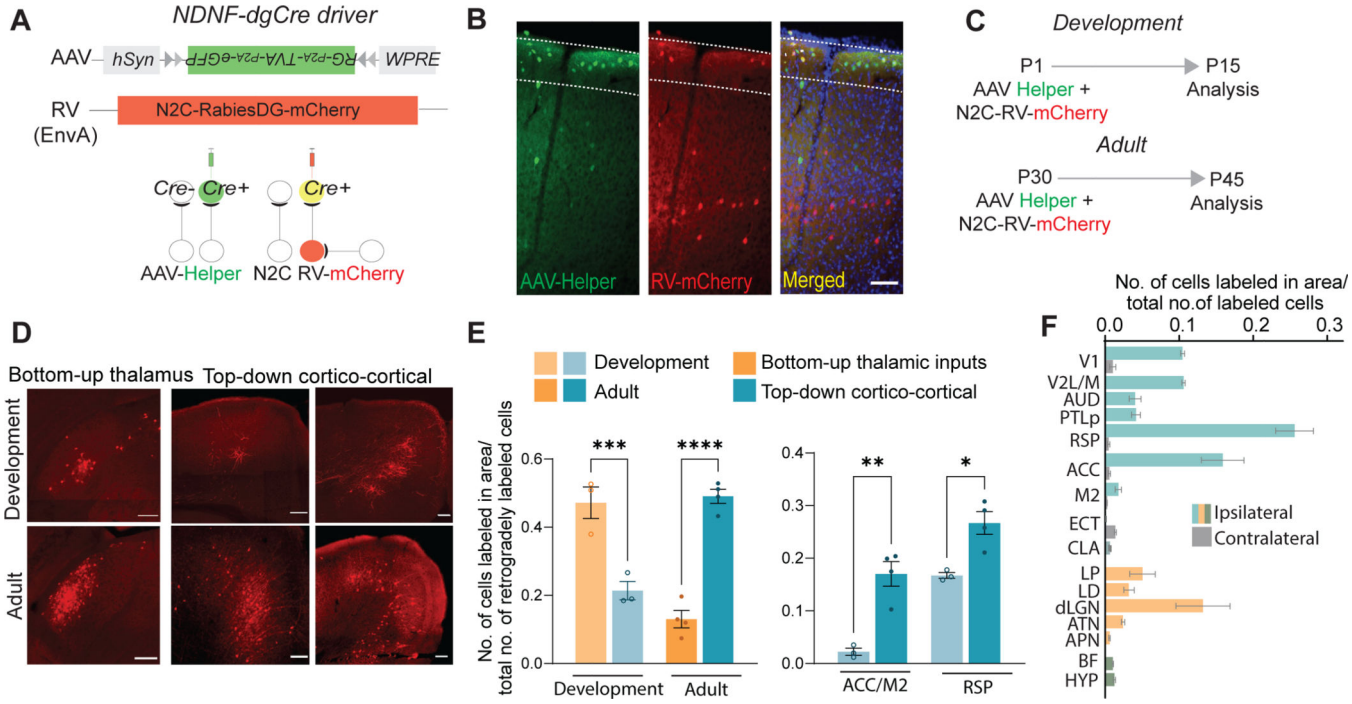

Fig. 1: Developing L1 INs switch from receiving predominantly bottom-up thalamic afferents to top-down cortico-cortical afferents

(A) Schematic of the monosynaptic rabies tracing strategy. Cre-dependent AAV-helper containing TVA, G protein and eGFP, was injected into the *NDNF-dgCre* driver line, followed by infection and retrograde labeling of an EnvA-pseudotyped CVS-N2c(ΔG) rabies virus (N2c-RV-mCherry, in red).

(**B**) Example image showing starter cell labeling in V1. AAV-helper-infected cells (eGFP, left panel), monosynaptically traced RV-mCherry (middle panel), and starter cells (arrowheads indicate GFP^+ and $mCherry^+$ labeled neurons in L1, right panel). Scale bar = 100μm

(C) Developmental timeline for early AAV-helper and N2c-RV-mCherry injections at two timepoints (top panel, developmental, P1 to P15; bottom panel, adult, P30 to P45).

(**D**) Examples of retrogradely labeled neurons from the dLGN (bottom-up thalamic inputs), ACC and RSP (top-down cortico-cortical inputs) at the developmental analysis timepoint, P15 (top row), and adult analysis time point, P45 (bottom row). Scale bar = 100μm

(E) Left panel: Quantification of the proportion of cells labeled normalized to the total number of labeled neurons in the brain (bottom-up thalamic vs top-down cortico-cortical) at development and adult time points (development bottom-up vs adult bottom-up. *p=<0.05; **p=<0.01, ***p=<0.005; One-way ANOVA with Tukey's correction for multiple comparisons). Right panel: Comparison of ACC/M2 and RSP inputs in development (light blue bars) and adults (dark blue bars). ****p=<0.001; One-way ANOVA with Tukey's correction for multiple comparisons (N=3 or 4 animals for each condition).

(**F**) Presynaptic inputs to L1 NDNF neurons in the adult V1 quantified as the number of cells labeled in each region divided by the total number of cells labeled in that brain. Colored bars represent ipsilateral connectivity, gray bars represent contralateral connectivity. Abbreviations: Cortex (Blue bars): Primary visual cortex (V1); Secondary visual areas

(V2L/M); Auditory cortex (AUD), Posterior parietal cortex (PTLp); Retrosplenial cortex (RSP); Anterior cingulate cortex (ACC); Secondary motor cortex (M2); Ectorhinal cortex (ECT); Claustrum (CLA). Thalamus (Orange bars): Lateral posterior nucleus (LP); Lateral dorsal nucleus (LD); dorso-lateral geniculate nucleus (dLGN); Anterior group of dorsal thalamic nuclei (ATN); Anterior pretectal nucleus (APN). Others (Green bars): Basal forebrain (BF-comprising Diagonal band NDB and Substantia Innominata SI); Hypothalamic nuclei (HYP-comprising lateral hypothalamic nucleus LHA, and preoptic are POA).

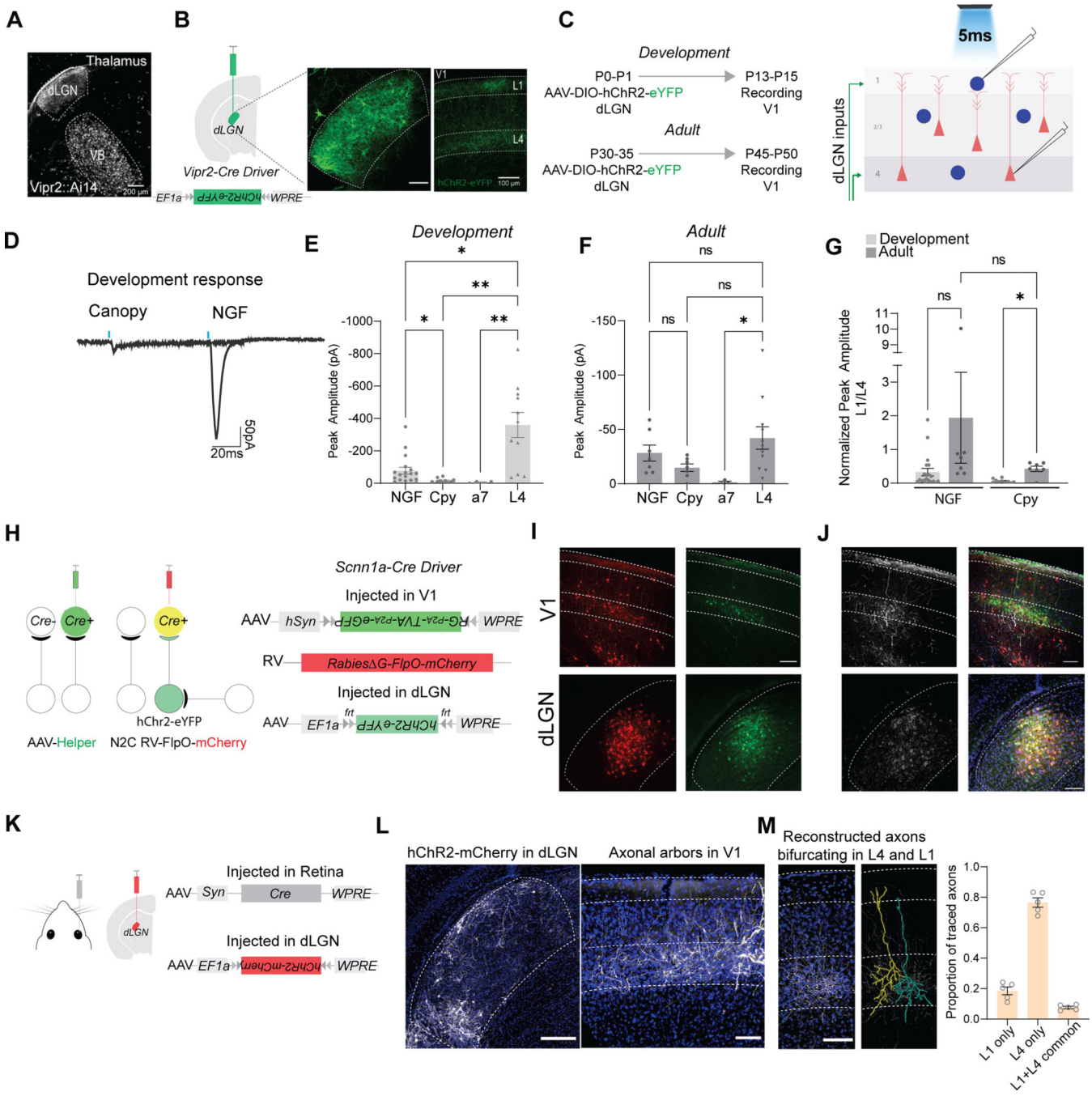

Fig 2: L1 NGF cells and L4 excitatory cells receive dLGN inputs, some of which are shared

(A) Image showing specificity for first-order thalamic nuclei dLGN and VB, using the *Vipr2-Cre* driver line crossed with Ai14 reporter line (Cre-dependent tdTomato) at P15. Scale bar = 200µm.

(**B)** Schematic of the AAV-DIO-hChr2-eYFP virus injection into dLGN of *Vipr2-Cre* driver line (left panel), virus expression in dLGN (middle panel) and resulting axonal projections to both L4 and L1 in V1 (right panel). Scale bar = 100µm.

(**C)** Left panel: Timeline for the AAV-DIO-hChr2-eYFP virus injection (P0–P1; P30–P35) and recording at development timepoint and adult timepoint (P13–P15; P45–P50). Right panel: Schematic of the slice recording to 5ms blue-light stimulation from L1 INs and L4 excitatory neurons in the same column.
(**D)** Example EPSC traces to blue light stimulation of dLGN fibers in V1 L1. Canopy cell response (left panel) and NGF cell response (right panel) from a P14 *Vipr2-Cre* mouse.
(**E)** Peak EPSC amplitude of all neurons recorded during development (NGF cells n=20; canopy cells n=10; alpha7 cells n=4; L4 cells n=10 from N=3–4 animals in each condition). One-way ANOVA with Tukey's correction for multiple comparisons; *p=<0.05; **p=<0.005
(**F)** Peak EPSC amplitude of all neurons recorded in adult. One-way ANOVA with Tukey's correction for multiple comparisons; *p=<0.05.
(**G)** L1 responses normalized to L4 responses in development and adult. One-way ANOVA with Tukey's correction for multiple comparisons; *p=<0.05.
(**H)** Modified FlpO-expressing RV approach to test whether L4 and L1 receive common inputs. Cre-dependent AAV-helper and N2c-RV-FlpO-mCherry viruses were injected in V1 of *Scnn1a-Cre* driver line, followed by flp-dependent AAV-fDIO-hChR2-eYFP virus injection in dLGN.
(**I)** Top left panel shows the N2c-RV-FlpO-mCherry expression in V1; top right panel shows the AAV-helper EGFP expression in L4 of V1.
(**J)** Antibody against hChR2 labeled fibers in V1 (top left panel), dLGN (bottom left panel) and merged images from I and J in V1 (top right panel) and the dLGN (bottom right panel). Scale bar = 100μm.
(**K)** Schematic to sparsely label neurons in dLGN. AAV-CamKII-Cre virus was injected in the right retina results in sparsely trans-synaptic cre expression in the dLGN, followed by an AAV-DIO-hChR2-mCherry virus injection in dLGN.
(**L)** Sparsely labeled neurons in dLGN (left panel), Scale bar = 500μm. dLGN fibers in V1 (right panel), Scale bar = 100μm.
(**M)** Left panel: Another example image showing sparsely labeled axons in both L4 and L1. Middle panel: Neurolucida tracing of dLGN axons reveals collaterals in L4 and L1. Right panel: Proportion of all axons traced (224 total axons from 5 confocal images across the anterior-posterior axis of V1).

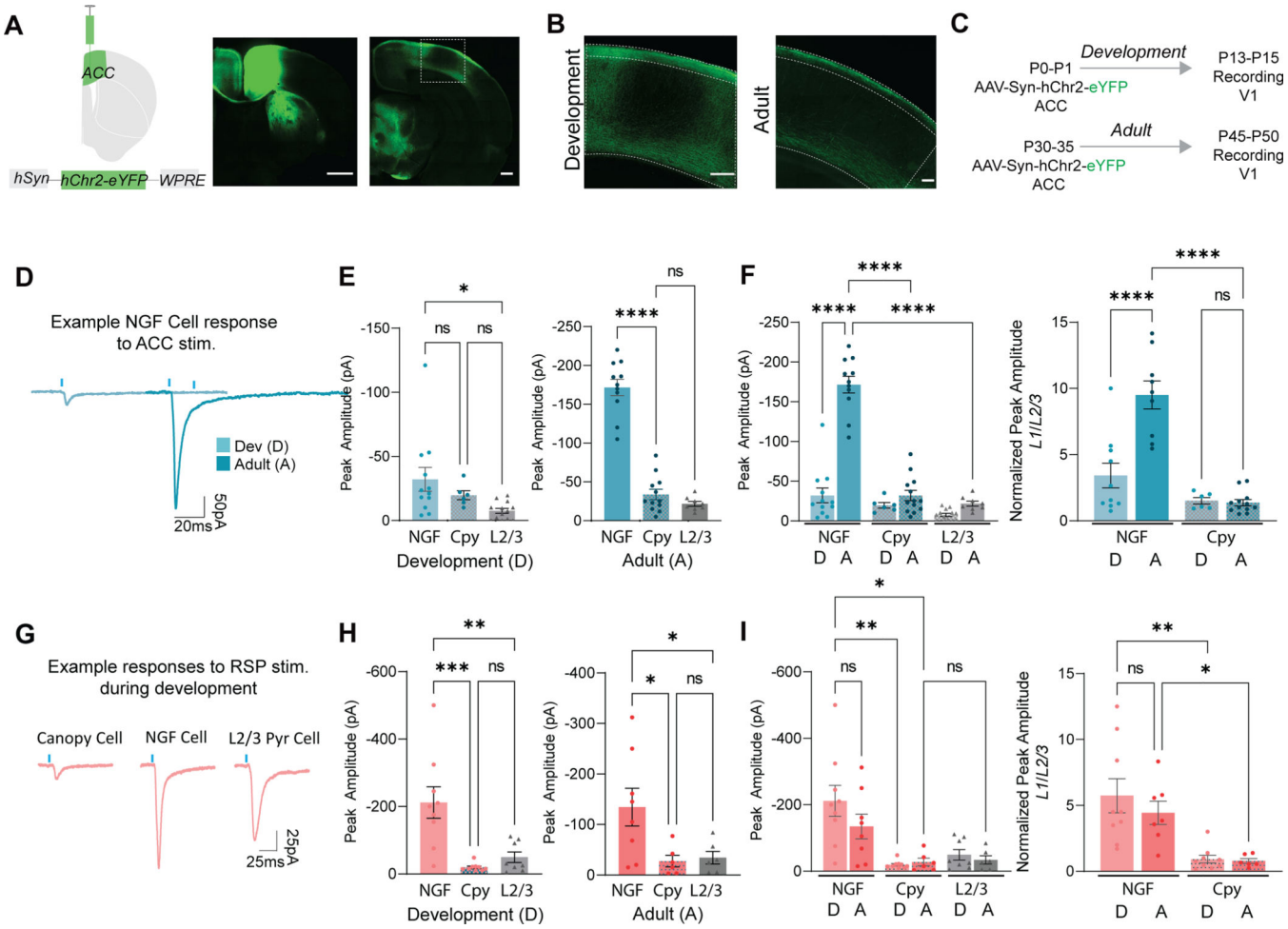

Fig. 3. ACC, but not RSP inputs to L1 INs strengthen across development

(A) Schematic of the hChR2-eYFP virus injection and eYFP expression in the ACC during development (left panel) and its axonal pattern in V1 (right panel). Scale bar = 500μm.

(B) Magnified view of the boxed region in A (left panel, development), and image of the axonal pattern in the adult V1 (right panel, adult). Scale Bar = 100μm.

(C) Timeline of virus injection in ACC and recording in V1 for both development and adult timepoints.

(D) Example traces of a NGF cell in V1 response to optogenetic stimulation of ACC fibers in development (left) and adult (right).

(E) Peak EPSC amplitude (to 5ms blue-light stimulation) of L1 NGF (n=12 cells from N=3 animals) and canopy (Cpy) (n=6 cells from N=3 animals) and L2/3 pyramidal neurons (n=13 cells from N=3 animals) during development (left) and in the adult (right) (NGF n=11 cells; canopy n=12 cells; L2/3 pyramidal, n=8 cells from N=4 animals). One-way ANOVA with Tukey's correction for multiple comparisons. *p=<0.05; ****p=<0.001.

(F) Pair-wise Comparison of the same data in E in development (D) and adult (A) (left panel) and same comparison after normalizing to L2/3 pyramidal neurons in the same slice (right) ***p=<0.005 ****p=<0.001 unpaired t-test

(G) Example traces of a canopy, NGF and a L2/3 pyramidal neuron in response to optogenetic stimulation of RSP fibers during development.
(H) Same as in E but for RSP stimulation (Development N=4 animals used; NGF: n=9 cells, canopy: n=8 cells; L2/3: n=8 cells; Adult N=3 animals used; NGF: n=8 cells, canopy n=6 cells, L2/3 n=6 cells). One-way ANOVA with Tukey's correction for multiple comparisons *p=<0.05; ***p=<0.005.
(I) Same as in F but for RSP stimulation. One-way ANOVA with Tukey's correction for multiple comparisons *p=<0.05; **p=<0.01.

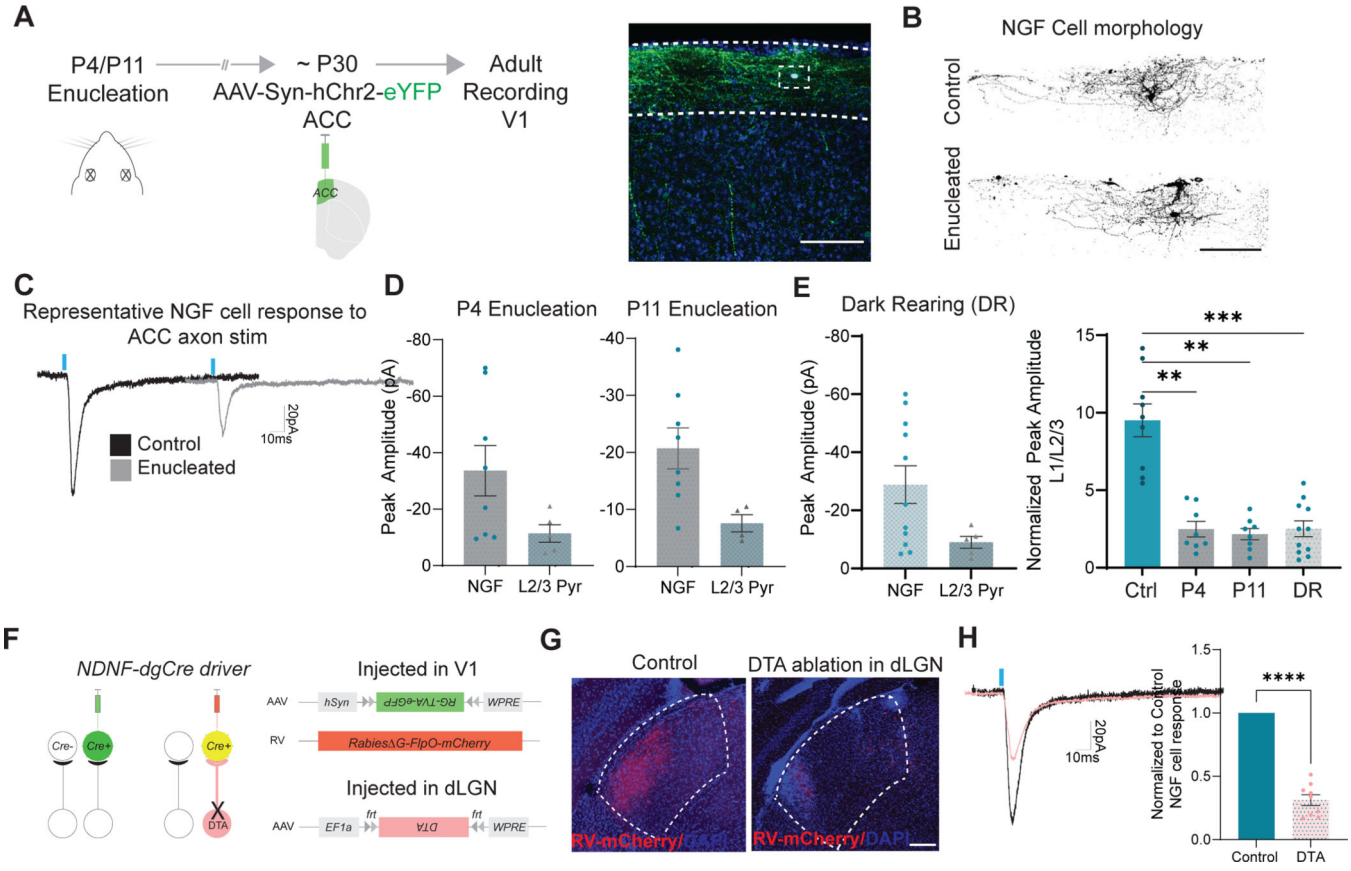

Fig. 4. L1 NGF cells require bottom-up sensory inputs for the strengthening of top-down connections

(A) Left, timeline of enucleation (either P4 or P11), Injection of AAV-hChr2 (~P30) into ACC and recording in L1 INs in V1 in adults (~P45). Right, example image showing ACC fibers in L1 in P4 enucleated mice. Boxed region shows a filled NGF cell. Scale bar = 100μm.

(B) Confocal images of recorded and filled neurogliaform cells in control (above) and P4 enucleated (below) mice. Enucleated cell is the boxed region in A. Scale bar = 100μm.

(C) Example traces of a NGF cell in response to optogenetic stimulation of ACC fibers in control (black) and enucleated (grey) animals.

(D) Comparison of peak amplitude responses (to 5ms stimulation) of NGF and L2/3 cells at P4 and P11 enucleation conditions to ACC fiber stimulation. Data points represent number of cells (n) from N=3–4 animals in each condition.

(E) Left, comparison of peak amplitude responses of NGF and L2/3 cells under dark rearing conditions (DR). Right, normalized peak amplitudes (to L2/3 pyramidal cells in same slice) for all sensory deprivation conditions. One-way ANOVA with Tukey's correction for multiple comparisons. *p=<0.05; **p=<0.01, ***p=<0.005.

(F) Schematic of the flp-dependent DTA ablation of L1 projecting dLGN axons. Cre-dependent AAV-helper and N2C-RV-FlpO-mCherry viruses injected in V1 of Ndnf-dgCre mouse; *Flp*-dependent AAV-fDIO-DTA injected in the dLGN. The timeline for DTA

ablations was similar to that in A (DTA injection at P4/5; ChR2 injection at P30; recording at ~P45).

(G) Example images showing DTA ablation in dLGN resulting in the elimination of most retrogradely neurons.Scale bar = 200μm

(H) Left, Example traces of a NGF cell in V1 response to optogenetic stimulation of ACC fibers in in control (black) and DTA-dLGN ablated afferents (pink) animals. Right, normalized responses of DTA experimental groups compared to wild type controls. ****p=<0.0001 unpaired t-test.

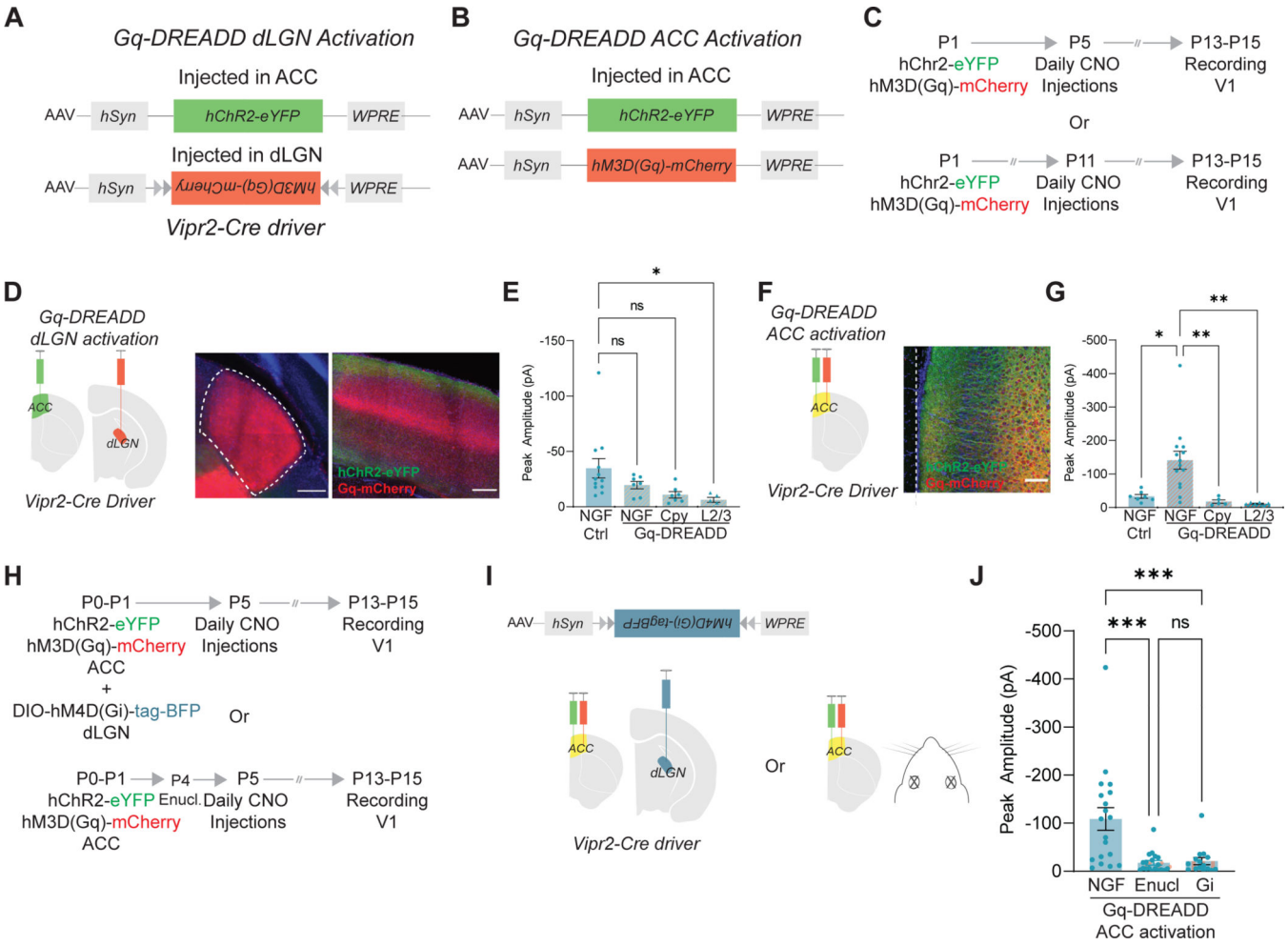

Fig. 5. Top-down connectivity onto L1 NGF cells depends upon coordination with bottom-up inputs

For Gq-DREADD dLGN activation: AAV-DIO-hM3D(Gq)-DREADD-mCherry was injected in the dLGN and hChR2-eYFP was injected in the ACC of Vipr2-Cre mice.

(A) For Gq-DREADD ACC activation: AAV-hM3D(Gq)-DREADD-mCherry and hChR2 eYFP were co-injected in the ACC of Vipr2-Cre mice.

(B) Timeline of AAV virus injection (P1), CNO administration (daily starting at P5) and recording of L1 INs in V1 (~P13–P15).

(C) Schematic of the Gq-DREADD dLGN-activation experiment (left panel), the expression of Gq-DREADD-mCherry in the thalamus (middle panel) and co-expression of Gq-DREADD-mCherry in the dLGN and hChR2-eYFP axons in V1 (right panel). Scale bar = 200μm.

(D) Comparison of peak EPSC amplitude response of the different cell types in V1 to ACC hChR2 stimulation: control vs Gq-DREADD dLGN activation. NGF=Neurogliaform cells; Cpy=Canopy Cells. Here the developmental control is same as in Fig 3E. One-way ANOVA with Tukey's correction for multiple comparisons ns=>0.05; *p=<0.05

(F) Schematic of the Gq-DREADD ACC-activation experiment (left panel) and co-expression of Gq-DREADD-mCherry and hChr2-eYFP in ACC (right panel). Scale bar = 100μm.

(G) Same as (E) but in CNO only control vs Gq-DREADD ACC activation. Cpy=Canopy Cells. One-way ANOVA with Tukey's correction for multiple comparisons *p=<0.05; **p=<0.01. ns comparisons not shown.

(H) Timeline of AAV virus injections (P1), CNO administration (daily starting at P5) recording in L1 INs in V1 (~P13-P15, top panel) or enucleation timeline (bottom panel).

(I) Schematic of the AAV-DIO-hM4D(Gi)-DREADD-tBFP dLGN-inhibition experiment, while simultaneously activating ACC with Gq-DREADD (left panel) and schematic of the enucleation combined with activation of ACC with Gq DREADD (right panels). In both experiments, ACC was injected with AAV-hChR2 as in E-F.

(J) Comparison of peak amplitude response of L1 NGF cells to hChR2 stimulation: Gq-DREADD ACC activation condition (same as in Fig 5G) vs Gq-DREADD ACC activation + enucleation condition (labeled as Enucl, middle bar) and Gq-DREADD ACC activation together with Gi-DREADD dLGN inhibition condition (labeled as Gi, right bar). One-way ANOVA with Tukey's correction for multiple comparisons ***p=<0.005

Table 1:

Key intrinsic physiological properties of NGF and canopy cells in V1 in development and in the adult.

	NGF Development	NGF Adult	Canopy Development	Canopy Adult
Resting Membrane Potential (mV)	−63.8 ± 0.25	−65.60 ± 1.12	−63.75 ± 0.5	−63.10 ± 0.6
Input Resistance (mOhm)	216.794 ± 2.8	282.24 ± 10.77	217.08 ± 4.84	223.01 ± 6.16
Sag Voltage deflection (mV)	−2.99 ± 0.07	−4.53 ± 0.26	−4.75 ± 0.24	−3.76 ± 0.301
First Spike Latency (ms)	529.22 ± 21.7	534.10 ± 54.28	73.56 ± 5.5	69.77 ± 8.99
Rheobase (pA)	124.28 ± 4.04	70.97 ± 6.94	107.5 ± 4.03	86.11 ± 5.32
AP Amplitude (mV)	50.67 ± 0.82	53.87 ± 2.18	49.42 ± 1.39	59.24 ± 2.07
AP Threshold (mV)	−22.80 ± 0.67	−32.82 ± 1.28	−27.67 ± 0.89	−34.24 ± 0.704
Rise Time (ms)	0.485 ± 0.006	0.442 ± 0.02	0.48 ± 0.015	0.417 ± 0.016
Decay Time (ms)	1.825 ± 0.025	1.69 ± 0.05	1.68 ± 0.024	1.55 ± 0.07
Half-Width (ms)	1.55 ± 0.03	1.41 ± 0.076	1.41 ± 0.039	1.25 ± 0.053
fAHP (mV)	−12.59 ± 0.59	−10.97 ± 1.17	−8.10 ± 0.64	−6.26 ± 0.75
mAHP (mV)	−21.56 ± 0.51	−16.61 ± 0.89	−13.81 ± 0.48	−9.40 ± 0.588

KEY RESOURCES TABLE

REAGENT or RESOURCE	SOURCE	IDENTIFIER
Antibodies		
Mouse monoclonal IgG2a anti-Channelrhodopsin 2	ARP	Cat# 03-651180, clone 1500; RRID:AB_2892521
Chicken anti-GFP	Aves labs	Cat# 1020 RRID:AB_10000240
Goat anti-mCherry	Sicgen	Cat# AB0040 RRID:AB_2333093
Donkey anti-chicken 488	Jackson Immunoresearch	Cat# 703-545-155 RRID:AB_2340375
Goat anti-mouse IgG2a 555	ThermoFisher Scientific	Cat# A-21137 RRID:AB_2535776
Donkey anti-goat 594	ThermoFisher Scientific	Cat# A-11058 RRID:AB_2534105
Streptavidin-647	ThermoFisher Scientific	Cat # S32357 RRID:AB_2892522
Guinee pig anti-NeuN	Millipore Sigma	Cat # ABN90 RRID:AB_11205592
Bacterial and virus strains		
AAV-DIO-N2C-G-P2A-TVA-P2A-eGFP	Pouchelon et al. 2020	N/A
EnvA-CVS-N2C(DG)-FlpO-mCherry	Pouchelon et al. 2020	N/A
AAV-hSyn-hChR2(H134R)-EYFP	Boyden, Zhang et al. 2005	Karl Deisseroth: Addgene_26973-AAV1 RRID:Addgene_26973-AAV1
AAV-EF1a-DIO-hChR2-eYFP	Boyden, Zhang et al. 2005	Karl Deisseroth: Addgene_20298 RRID:Addgene_20298
AAV-hSyn-fDIO-DTA	This paper	N/A
AAV2/1-Ef1a-fDIO-hChr2-eYFP	Fenno, Mattis et al. 2014	Karl Deisseroth: Addgene_55639 RRID:Addgene_55639
pENN-AAV2/1-CamKII-Cre.SV40	Gift from James Wilson	James Wilson: Addgene_105558 RRID:Addgene_105558
AAV (PHP-eB)-S5E2-GFP	Vormstein-Schneider, Lin et al. 2020	Jordane Dimidschtein: Addgene_135631 RRID:Addgene 135631
hSyn-DIO-hM4D(Gi)-tagBFP	This paper	N/A
AAV-hSyn-DIO-hM3D(Gq)-mCherry	Krashes, Koda et al. 2011	Bryan Roth: Addgene_44361-PHP-eB RRID:Addgene_44361-PHP-eB
AAV-hSyn-hM3D(Gq)-mCherry	Gift from Bryan Roth	Bryan Roth: Addgene_50475-AAV2 RRID:Addgene_50475-AAV2
Chemicals, peptides, and recombinant proteins		
Clozapine-N-Oxide	Tocris Bioscience	Cat. No. 4936
Tetrodotoxin	Tocris Bioscience	Cat. No. 1078
4-Aminopyridine	Tocris Bioscience	Cat. No. 0940
Experimental models: Organisms/strains		
Mouse: B6.Cg-*Ndnf*$^{tm1.1(folA/cre)Hze}$/J	Jackson Laboratories	Cat. No. 028536 RRID:IMSR_JAX:028536
Mouse: B6.Cg-*Vipr2*$^{em1.1(cre)Hze}$/J	Jackson Laboratories	Cat. No. 031332 RRID:IMSR_JAX:031332
Mouse: B6.Cg-*Gt(ROSA)26Sor*$^{tm14(CAG-tdTomato)Hze}$/J	Jackson Laboratories	Cat. No. 007914 RRID:IMSR_JAX:007914
Mouse: B6;C3-Tg(Scnn1a-cre)3Aibs/J	Jackson Laboratories	Cat. No. 009613 RRID:IMSR_JAX:009613
Mouse: B6.FVB-Tg(Npy-hrGFP)1Lowl/J	Jackson Laboratories	Cat. No. 006417 RRID:IMSR_JAX:006417
Mouse: B6 *Sst*$^{tm2.1(cre)Zjh}$/J	Jackson Laboratories	Cat. No. 013044 RRID:IMSR_JAX:013044
Mouse: B6. *Vip*$^{tm1(cre)Zjh}$/J	Jackson Laboratories	Cat. No. 010908 RRID:IMSR_JAX:010908

REAGENT or RESOURCE	SOURCE	IDENTIFIER
Mouse: B6;129-*Gt(ROSA)26Sor*$^{tm5(CAG-Sun1/sfGFP)Nat}$/J	Jackson Laboratories	Cat. No. 021039 RRID:IMSR_JAX:021039
B6.129P2-*Pvalb*$^{tm1(cre)Arbr}$/J	Jackson Laboratories	Cat. No. 017320 RRID:IMSR_JAX:017320
Recombinant DNA		
CVS-N2c(DG)-mCherry-P2A-FlpO	Reardon, Murray et al. 2016	Thomas Jessel; Addgene_73471 RRID:Addgene_73471
VTKS1 backbone	NYUAD	Addgene_170852
VTKS2 backbone	NYUAD	Addgene_170853
VTKS3 backbone	NYUAD	Addgene_170854
Software and algorithms		
Clampfit 10.7 (pClamp)	Molecular Devices	http://www.moleculardevices.com/products/software/pclamp.html RRID:SCR_011323
Easy Electrophysiology V2	Easy Electrophysiology	http://www.easyelectrophysiology.com RRID:SCR_021190
Prism 9.1.2	Graphpad Software	http://www.graphpad.com/ RRID:SCR_002798
Zen Blue 2.6	Zeiss	http://www.zeiss.com/microscopy/en_us/products/microscope-software/zen.html#introduction RRID:SCR_013672
Neurolucida 360	MBF Bioscience	https://www.mbfbioscience.com/neurolucida360 RRID:SCR_016788
ImageJ 2.0.0 Java 1.8.0_66	National Institute of Health	https://imagej.net/ RRID:SCR_003070